UNESCO Chair on Coastal Geo-Hazard Analysis
Research Institute for Earth Sciences
Geological Survey of Iran

Abstract:

At the request of the Research Institute of Earth Sciences affiliated to the Geological Survey of Iran, geophysical surveys were carried out for tectonic and sedimentological studies in the protected area of Miankaleh, Mazandaran. In this study, magnetometry, electrical resistivity and Ground-Penetrating Radar (GPR) methods have been used for subsurface investigations. Totally, 1489 data by magnetometry method, 3523 data by electrical resistivity method and 5500 linear meters of GPR data were collected in 6 profiles. The Miankaleh Peninsula is located in the southeast of the Caspian Sea and on the border of Mazandaran and Golestan provinces. In this study 6 profiles with approximate south-north trend carried out in Miankaleh Peninsula.

ISBN: 978-622-5858-76-3

2024

UNESCO Chair on Coastal Geo-Hazard Analysis
Research Institute for Earth Sciences
Geological Survey of Iran

Geoelectric, Magnetometry and ground-penetrating radar studies for tectonic and sedimentology investigation in Miankaleh region (Mazandaran province)

UCCGHA 020

2024

Geoelectric, magnetometry and ground-penetrating radar studies for tectonic and sedimentology investigation in Miankaleh region (Mazandaran province)

سرشناسه : محمدی‌ویژه، مهدی، ۱۳۶۰-
-Mohammadi vizheh, Mehdi, 1982

عنوان و نام پدیدآور : Geoelectric, magnetometry and ground-penetrating radar studies for tectonic and sedimentology investigation in Miankaleh region (Mazandaran province)[Book]/ authors Mehdi Mohammadi Vizheh, Hosain Iranshahi, Hesam gholami; supervisor Hamid Nazari; employer Geological survey of Iran; advisor Research Institute for Earth Sciences; summarized and translated into English Manouchehr Ghorashi; with cooperation UNESCO Chair on Coastal Geo-Hazard Analysis.

مشخصات نشر : تهران: نشر خزه، ۱۴۰۲= ۲۰۲٤ م.

مشخصات ظاهری : ۱۲۴ص.؛ ۱۴/۵ × ۲۱/۵ س‌م.

شابک : 978-622-5858-76-3

وضعیت فهرست نویسی : فیپا

یادداشت : زبان: انگلیسی.

آوانویسی عنوان : ژئوالکتریک -- مگنتومتری

موضوع : ژئوفیزیک -- ایران -- مازندران

موضوع : Geophysics -- Iran -- Mazandaran

موضوع : زمین‌شناسی ساختاری -- ژئوالکتریک – مگنتومتری -- میانکاله

موضوع : Structural Geology -- Geoelectric – Magnetonetry -- Miankaleh

شناسه افزوده : ایرانشاهی، حسین، ۱۳٦۰

شناسه افزوده : iranshahi, Hosain, 1981-

شناسه افزوده : غلامی، حسام، ۱۳۵۳

شناسه افزوده : gholami, Hesam, 1974-

شناسه افزوده : نظری، حمید، ۱۳۴۶-، ناظر

شناسه افزوده : Nazari, Hamid, 1968-

شناسه افزوده : قرشی، منوچهر، ۱۳۲۰-، مترجم

شناسه افزوده : Ghorashi, Manouchehr- 1941

شناسه افزوده : یونسکو. کرسی مخاطرات زمین شناختی ساحلی

شناسه افزوده : UNESCO Chair on Coastal Geo-Hazard Analysis

شناسه افزوده : سازمان زمین‌شناسی و اکتشافات معدنی کشور

شناسه افزوده : Geological Survey of Iran

شناسه افزوده : سازمان زمین‌شناسی و اکتشافات معدنی کشور. پژوهشکده علوم زمین

شناسه افزوده : Geological Survey of Iran. Research Institute for Earth Sciences

رده بندی کنگره : QE۶۰۱/م۳ج۹ ۱۴۰۲

رده بندی دیویی : ۸۰۹۵۵۲۲/۵۵۱

شماره کتابشناسی ملی : ۹۴۷۴۸۲۶

Geoelectric, magnetometry and ground-penetrating radar studies for tectonic and sedimentology investigation in Miankaleh region (Mazandaran province)

Author:

Mehdi Mohammadi vizheh

نشرخزه

اطلاعات گزارش

عنوان: مطالعات ژئوالکتریک، مغناطیس سنجی و رادار نفوذی به زمین برای بررسی های تکتونیک و رسوب شناسی در محدوده میانکاله (استان مازندران)

مجری: سازمان زمین‌شناسی و اکتشافات معدنی کشور

مشاور: پژوهشکده علوم زمین

زبان مرجع: فارسی

خروجی: گزارش، نقشه، مقاله، داده های الکترونیکی

ناظر علمی: حمید نظری

نویسندگان: مهدی محمدی ویژه، حسین ایرانشاهی، حسام غلامی

رئیس کرسی یونسکو در مخاطرات زمین شناختی ساحلی: حمید نظری

مسئول شورای اجرایی: راضیه لک

خلاصه‌نویسی و ترجمه به انگلیسی: منوچهر قرشی

خلاصه شده از: طرح مخاطرات زمین شناسی دریایی حوضه جنوب کاسپین

ناشر: نشر خزه

با همکاری کرسی یونسکو در مخاطرات زمین شناختی ساحلی

چاپ اول: ۱۴۰۲

شمارگان: ۵۰ نسخه

صفحات: ۱۲۴

شابک: ۹۷۸-۶۲۲-۵۸۵۸-۷۶-۳

khazepub@gmail.com

Report Information

Title: Geoelectric, magnetometry and ground-penetrating radar studies for tectonic and sedimentology investigation in Miankaleh region (Mazandaran province)

Employer: Geological survey of Iran

Advisor: Research Institute for Earth Sciences

Original language: Persian

Output: Report, Map, Paper, Digital Meta Data

Supervisor: Hamid Nazari

Authors: Mehdi Mohammadi vizheh, Hossein Iranshahi, Hesam Gholami

Chairholder in the UNESCO Chair on Coastal Geo-Hazard Analysis: Hamid Nazari

Head of the Executive Council: Razyeh Lak

Summarized and translated into English: Manouchehr Ghorashi

Summarized after: Geohazard South Caspian Carpet (GSCC)

Publisher: Khazeh Publication

with cooperation UNESCO Chair on Coastal Geo-Hazard Analysis

First Edition: 2024

Edition number: 50

Page: 124

Shabak: 978-622-5858-76-3

khazepub@gmail.com

Scientific Council

Name	Affiliation
Ara Avagyan	IGS: Institute Geological Sciences
Rick J Bailey	IOC-UNESCO Indian Ocean Tsunami Warning and Mitigation System/ UNESCO
Aram Fathian Baneh	University of Calgary
Wenjiao Xiao	Chinese Academy of Sciences
Magdi Guirguis	Institut français d'archéologie orientale du Caire
Richard Walker	University of Oxford
Philippe Agard	University of Sorbonne
Justin Ahanhanzo	Intergovernmental Oceanographic Commission of UNESCO (IOC-UNESCO)
Alice Aurelie	UNESCO Water Sciences Division
Eric Barrier	University of Sorbonne
Jean-François Ritz	University of Montpellier
Martin Hanz	German under water archaeology association
Klaus Reicherter	Aachen University
Judith Thomalsky	German Archaeological Institute Tehran Branch
Hamid Alizadeh Lahijani	Iranian National Institute for Oceanography and Atmospheric Science
Abbas Banj Shafiei	Urmia University
Yahya Djamour	Shahid Beheshti University (SBU)
Hassan Fazeli Nashli	University of Tehran
Razyeh Lak	Research Institute for Earth Sciences
Mohammad Mokhtari	International Institute of Earthquake

	Engineering and Seismology
Hamid Nazari	Research Institute for Earth Sciences
Jafar Omrani	Geological Survey of Iran
Morteza Talebian	Research Institute for Earth Sciences
Mohammad Tatar	International Institute of Earthquake Engineering and Seismology
Mahdi Zare	International Institute of Earthquake Engineering and Seismology
Stefano Salvi	National Institute of Geophysics and Volcanology (INGV)
Ryo Anma	Tokushima University
Yeong Bae Seong	Korea University
John Lambert	Deltares, UNESCO
Issa El-Hussain	Sultan Qaboos University
Ekkehard Holzbecher	German University of Technology in Oman
Egor Krasinskiy	Underwater research center Russian Geographical Society
Audemard Franck A.	Department of Geology, Central University of Venezuela
Executive Committee	
Name	**Affiliation**
Nasir Ahmadi	Environmental Protection Organization of Mazandaran Province
Arash Amini	Golestan University
Alireza Amrikazemi	Scientific Coordinator, Qeshm Island UNESCO Global Geopark
Parviz Armani	Imam Khomeini International University
Ataollah Dadashpour	Geological Survey of Iran, Sari branch

Asghar Dolati	Kharazmi University
Hasan Fazelinashli	University of Tehran
Fahimeh Foroghi	Iranian National Institute for Oceanography and Atmospheric Science
Abdolazaim Ghanghormeh	Golestan University
Habibolah Ghasemi	Shahrood University of Technology
Mohammad reza Ghasemi	Research Institute for Earth Sciences
Manouchehr Ghorashi	Research Institute for Earth Sciences
Jafar Hassanpour	University of Tehran
Ataollah Kavian	Environmental Protection Organization of Mazandaran Province
Mohammadreza Kazemzadeh	Superme Audit Gourt
Razyeh Lak	Head of RIES and Executive Manager
Mahmoudreza Majidifard	Research Institute for Earth Sciences
Ali Akbar Momeni	Shahrood University of Technology
Babak Moradi	Iranian National Institute for Oceanography and Atmospheric Science
Seyed Mohsen Mortazavi	Hormozgan University
Hasan Nasrollah Zadeh Saravi	Caspian Sea Ecological Research Center
Ehsan Pegah	Kharazmi University
Abdolwahed Pehpouri	Qeshm Island UNESCO Global Geopark
Ahmadreza Rabani	University of Science and Technology of Mazandaran
Mahdi Rahmanian	Shargh Daily newspaper
Ahmad Rashidi	International Institute of Earthquake Engineering and Seismology
Masoud Sadri Nasab	University of Tehran
Mohammad Salamati	Respina Company

Mohammad Tatar	International Institute of Earthquake Engineering and Seismology
Alireza Vaezi	Research Institute for Earth Sciences
Mojtaba Yamani	University of Tehran
Ahmed Hadidi	German University of Technology in Oman (GUTECH)
Secretariat	
Name	**Affiliation**
Elnaz Aghaali	Research Institute for Earth Sciences
Keivan Ajdari	Research Institute for Earth Sciences
Hourieh AliBeygi	Research Institute for Earth Sciences
Sedigheh Ghanipour	Research Institute for Earth Sciences
Hamoon Memarian	Research Institute for Earth Sciences
Shirin Safavi	Research Institute for Earth Sciences
Aazam Takhtchin	Research Institute for Earth Sciences
Mehrnoosh Pour Saeid	Graphic Designer
Hanieh Bakhshaei	Geological Survey of Iran
Reza Behbahani	Geological Survey of Iran
Javad Darvishi khatooni	Geological Survey of Iran
Mohammadreza Ensani	Geological Survey of Iran
Marziyeh Estrabi Ashtiyani	Geological Survey of Iran
Gholamreza Hoseinyar	Geological Survey of Iran
Mojtaba Kavianpour Sangno	Geological Survey of Iran

Contents

Table of Figures

Table of Table

Chapter 1

General

1-1- Introduction

At the request of the Research Institute of Earth Sciences affiliated to the Geological Survey of Iran, geophysical surveys were carried out for tectonic and sedimentological studies in the protected area of Miankaleh, Mazandaran. In this study, magnetometry, electrical resistivity and Ground-Penetrating Radar (GPR) methods have been used for subsurface investigations. Totally, 1489 data by magnetometry method, 3523 data by electrical resistivity method and 5500 linear meters of GPR data were collected in 6 profiles.

1-2- Geographical location of the studied areas

The Miankaleh Peninsula is located in the southeast of the Caspian Sea and on the border of Mazandaran and Golestan provinces. In this study 6 profiles with approximate south-north trend carried out in Miankaleh Peninsula. Figure 1 &Figure 2 show the access roads around the Miankaleh Peninsula and the

position of the studied profiles on the satellite image of the survey area.

1-3- Brief geology of Miankaleh Peninsula

The Miankale Peninsula is located in the Behshahr, Geological map, scale 100,000 and most the investigated area is covered with recent sedimentary deposits, such as coastal and aeolian sand, silts and clay deposits (Figure 3 & Figure 4). In Figure 3, the location of profiles in the Miankaleh Peninsula is shown on the 1:100,000 geological map of Behshahr.

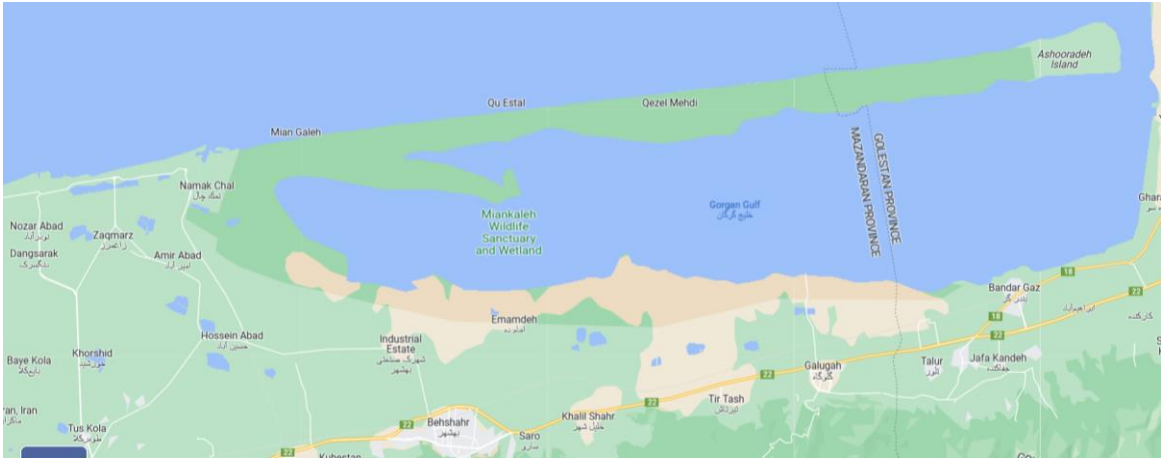

Figure 1: The general location of the Miankaleh Peninsula on the road map

Figure 2: The general location of the collected profiles (black lines) on the satellite image (taken from Google earth software) of the studied area.

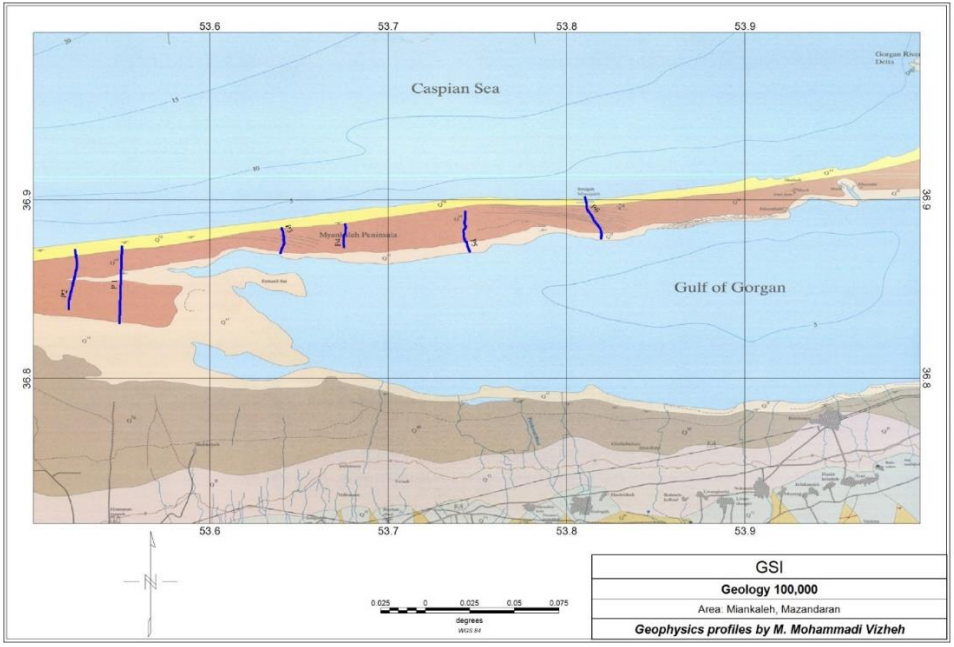

Figure 3: The location of geophysical profiles (blue lines) on a part of the 1:100,000 geological map of Behshahr (Ghasemi et al., 2002).

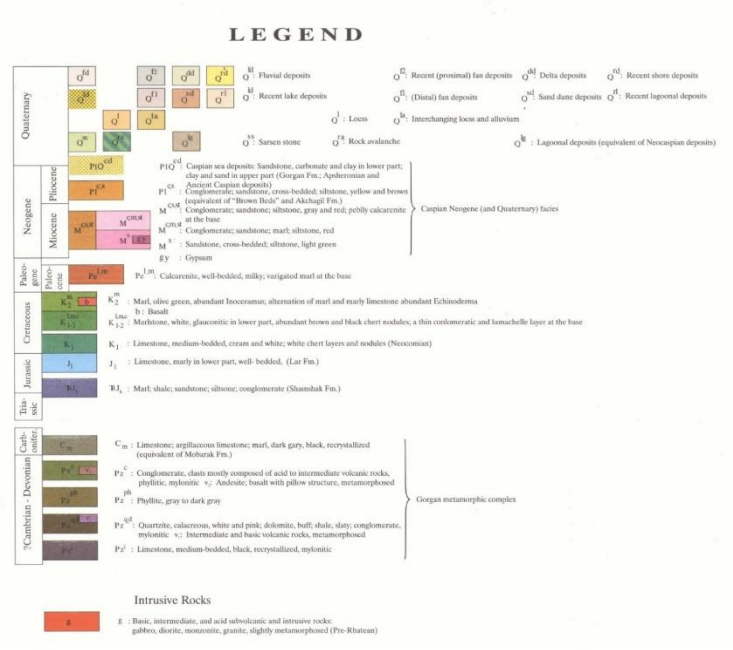

Figure 4: Legend of Behshahr geological map, scale 1:100,000

Chapter 2

Geophysical methods

In this chapter, the theory of geophysical methods used in this study is briefly presented.

2-1- Electrical resistivity method

The electrical surveys, detect surface traces resulting from the passage of current inside the earth. Compared to other geophysical methods such as gravimetry, magnetometry, and radioactivity, in which only one force field or anomalous feature is used, electrical methods have more variety than other geophysical methods. The main purpose of electrical methods is to measure the electrical resistivity of the earth. In order to identify a subsurface feature, its electrical resistivity must be significantly different from its surrounding environment. Therefore, the use of electrical methods is limited to cases where there is a resistivity variation. In these methods, geological features, underground water and other existing features are not measured directly. But for proper interpretation of electrical data, a series of external information is needed.

Direct-current (DC) resistivity method, which is one of the well-known geoelectrical methods, is effectively used to discover underground water resources, investigate groundwater pollution, reveal the location of subsurface cavities, faults and crushed zones, as well as buried archeological sites. The target of resistivity measurements is to determine the underground distribution of resistivity by surface measurements. Based on these measurements, the actual resistivity of subsurface structures can be estimated.

By injecting current into the ground through two current electrodes and measuring the resulting voltage difference between two potential electrodes, the resistivity of subsurface structures can be estimated. Figure 5 shows a four-electrode array. A and B electrodes are current electrodes and M and N electrodes are potential electrodes. Following equation is the basic equation for calculating the apparent resistivity for any type of electrode arrangement.

$$\rho_a = \frac{2\pi}{\left\{\left(\frac{1}{AM}-\frac{1}{BM}\right)-\left(\frac{1}{AN}-\frac{1}{BN}\right)\right\}}\frac{\Delta V}{I}$$

In this regard, I is the intensity of the transmitted current (in amperes), ΔV, is the potential difference (in volts) and ρ_a is the value of apparent resistivity (in Ωm). If the ground is inhomogeneous (which is usually is the same) and the electrode distances change, or if the distances are fixed while the arrangement changes, the resistivity will change completely. The result is that in each measurement, a different_apparent resistivity is obtained. It is clear that the magnitude of this value is closely related to the arrangement of the electrodes. Although this apparent resistivity to some extent characterizes the real regional resistivity near the set of electrodes, but, it will definitely not be an absolute value.

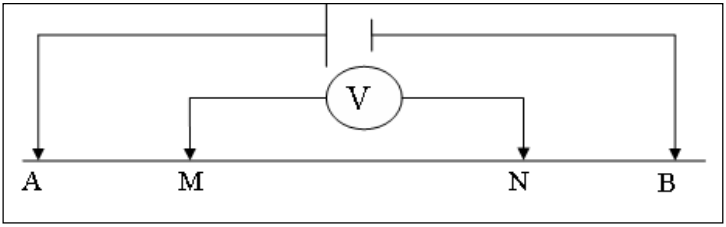

Figure 5: Arrangement of four electrodes

The relationship between real and apparent resistivity is a complex relationship. To determine the real resistivity of subsurface structures from its apparent

values, inversion methods are used by computer software and codes.

2-1-1- Resistivity of subsurface structures

Resistivity measurements provide the resistivity changes of subsurface structures. To convert these images into geological images, information about resistivity values of various types of subsurface structures as well as the geology of the area under investigation is important. The resistivity of some materials and rocks are given in Table 1. The range of resistivity changes is much higher compared to the physical quantities that are calculated in other geophysical methods. The electrical resistivity of different materials varies from 1.6×10^{-8} Ωm for pure silver to 10^{16} Ωm for pure sulfur. Metamorphic and igneous rocks usually have high resistivity values. The resistivity of metamorphic and igneous are high and their resistivity basically dependent on the degree of fracture and their percentage of subsurface water filling.

Sedimentary rocks usually have a low resistivity due to their porosity and higher water content. Wet soils and fresh underground waters have low resistivity. Clay soils have lower resistivity than sands. The resistivity of sea water, which is equal to the 0.2 Ωmeter, is result of the high amount of dissolved salts.

As can be seen in Table 1, there is resistivity overlaps between most types of rocks and soils. This matter comes from the fact that the resistivity of particular specimens of soil and rock depends on several different factors. The effective factors in their specific electrical resistance are:

- Stone porosity and the amount of fractures
- The position of the pores of the stone
- A volume of rock pores that contains water
- Electrical conductivity of the water in the rock
- The type of minerals that constitute the rock

Therefore, the resistivity of a layer depends on the geological condition of the studied area. In other words, it is not possible to separate the layers, only according to their geological characterizes, that is, in order to obtaining the resistivity, of sediments, formations and geological units in each region must be determined separately.

Table 1: resistivity of some types of water, rock and sediments

Geological material	Resistivity (ohm meter)
Asmari limestone	-500 > 1000
Cretaceous limestone	200 – 500
Quartzite	300 – 10000
Volcanic ash	20 – 100
Underground water	10 – 100
Sea water	0.2
Limestone	50 – 5000
Shale	20 – 2000
Clay	1 – 100
Course-grained alluvium and conglomerate	300 – 10000
Medium-grained alluvium	100 – 300
Fine-grained alluvium	50 – 100
Dried sand and gravel	1000 – 10000
Water saturated sand and gravel	50 – 500
Brine saturated sand and gravel	0.5 - 5

2-1-2- Methods of measuring resistivity data

Resistivity data are obtained in one-dimensional, 2D, and three-dimensional forms. A geoelectric operation is done either by vertical electric sounding (VES) or profiling. In the sounding method, depth or vertical variations of resistivity are studied. But in the

profiling method, lateral changes of the resistivity of subsurface materials along a profile line are investigated. In the profiling method, the array and its parameters remain constant and the electrodes are displaced along the profile line. While there are lateral and subsurface changes in resistivity along the length of the investigated profile, the data are collected in two or three dimensions (combination of sounding and profiling).

2-1-3- Electrode arrays

Various electrode array has been proposed for resistivity measurements. The most important array used in the resistivity method, are Wenner, Schlumberger, dipole-dipole.

As mentioned earlier, dipole-dipole and pole-dipole arrays were used in this study. In dipole-dipole array, all four electrodes A, B, M, N are located along one profile, and actually the distance of the transmitter electrodes is equal to the distance of the receiver electrodes and is equal to a constant value of a *(AB=MN=a)*. In each measurement, the AB electrodes are fixed and the MN electrodes move along the profile. The distance between the nearest current and potential electrodes is equal to *na (n=1,2,3,...)* and the depth of each measurement will be equal to *(n+1)a/2*. The measured number is attributed to a point at the intersection of two lines with an angle of 45 degrees

compared to the surface of the earth drawn from the middle of AB, MN. In this way, from the total points measured by this method, a pseudo-section of apparent resistivity along a profile will be obtained (Figure 6). It is worth noting that the depth obtained from this method is not the real depth and different modelling methods are used to achieve more realistic depths.

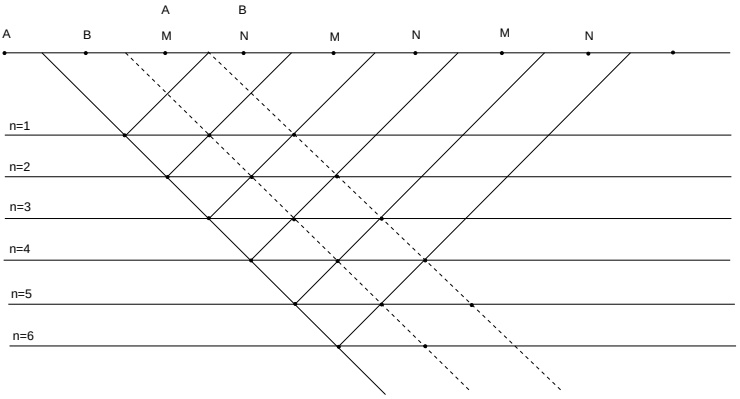

Figure 6: Dipole-Dipole array

2-2- Magnetometery method

The study of the earth's magnetism is the oldest branch of geophysics, which has been used for many years in the exploration of oil, economic minerals, and even archaeological purposes. For the first time, Gilbert

showed that the earth's magnetic field has a generally north-south direction near the earth's rotation axis. Since then, significant progress has been made in the field of making equipment and interpreting the measurements of this method. Magnetic surveying is done based on the measurement of magnetic field changes in the studied area. In fact, magnetic exploration can be considered a combination of mathematical, physical and geological sciences. In magnetic methods, the total field or vertical component is usually measured. Due to the fact that the magnetic field has two poles and also a trend, therefore, the interpretation of the results is more complicated than other methods. On the other hand, compared to most geophysical methods, field measurements of magnetometry are cheap and simple, and there is practically no need to apply complex and long corrections in the readings.

As far as exploration geophysics is concerned, the Earth's magnetic field consists of three parts:

1. The main field, which, although not constant with time, changes relatively slowly and its origin is internal and constitutes about 90% of the Earth's magnetic field.
2. Crustal field, which depends on the variation of magnetic ore content of rocks near the surface of the Earth's crust.

3. The external field is a small part of the main field that originates outside the earth and changes relatively quickly, a change that is partly periodic and partly random (related to the daily and annual changes of the sun and the moon).

Variations of the main field are usually but not always much smaller than the main field, and are relatively constant with time and space, and arise from local magnetic anomalies near the surface of the Earth's crust. These changes constitute the goals of exploration geophysics.

If an object is placed in the earth's field F, then a field called J (induced magnetization) is induced inside the object,

$$J = KF$$

where K is the susceptibility. Objects are divided into three categories according to the K factor:

- $K<0$, Diamagnetism. The most common diamagnetic materials of the earth are graphite, gypsum, marble, quartz and salt.
- $K>0$, Para magnetism. Elements such as nickel and calcium, etc., this effect decreases with temperature.
- $K>>0$, Ferromagnetism is mostly iron oxides.

Susceptibility is an important variable in magnetism and plays the same role as density in gravity interpretations. Although there are large variations in *K* values, even for a particular rock, and a wide overlap between different types is observed, but sedimentary rocks have the lowest and igneous rocks have the highest average susceptibility. In each case, the susceptibility depends only on the amount of ferromagnetic minerals, which are mainly magnetite and sometimes Ilmenite or Pyrrhotite. For instance, igneous rocks such as gabbro, pyroxenite, basalt and andesite have high magnetic susceptibility.

It is often possible to determine minerals with negative susceptibility by detailed magnetic measurements, although these negative values are small. It should also be noted that many iron minerals are only slightly magnetic. Rocks and minerals are divided into three categories in terms of magnetism; Diamagnetic (without magnet), paramagnetic (with magnet when exposed to a magnetic field) and ferromagnetic (with magnet) (Telford et al., 1990).

The parameter for measuring the magnetic properties of rocks is the magnetic susceptibility, which is presented in Table 2 for a number of minerals. This quantity in the *emu* system is a dimensionless quantity and its value is 4π times its value in the *SI* system (Blakely, 1995).

Table 2: Average susceptibility of some rocks and minerals (Telford et al., 1990)

Type	**Average susceptibility (SI) × 10^3**	**Type**	**Average susceptibility (SI) × 10^3**
Hematite	6.5	Chromite	7
Magnetite	6000	Limonite	2.5
Coal	0.02	Quartz	-0.01
Andesite	160	Limestone	0.3

2-3- Theory of GPR method

GPR is one of the geophysical methods for surveying near the ground surface. In this method, high frequency electromagnetic waves (in the range of 10 to 2500 MHz) used to detect subsurface structures. GPR equipment reveal subsurface discontinuities with high resolution by producing and emitting discontinuous electromagnetic pulses. These pulses are produced by the signal generator and sent into the ground by different antennas. The shape and characteristics of the produced pulses are a function of the characteristics of the antennas that are used for surveying, and these antennas are generally named according to the frequency center of the produced pulse.

In general, the success of geophysical methods depends on the contrast in the physical characteristics of subsurface targets with their surrounding environment. In most geological conditions, where the conductivity and magnetic permeability of the subsurface environment can be ignored, the contrast in dielectric transmissivity has the greatest contribution in detecting subsurface targets by GPR method. Therefore, by using this method, many subsurface anomalies can be detected. The range of GPR applications is very wide and for various purposes such as determining the thickness of the soil as well as the stratigraphy of sediments, determining the water table, detecting buried holes,

channels and tunnels, detecting fractures and cracks in dense rocks. , mapping contaminated areas in environmental studies, investigating the conditions of construction sites of huge structures, non-destructive testing of building materials, bridge pillars and dam walls, revealing buried objects in archaeological investigations, revealing construction facilities such as buried cables and pipes, determining the thickness of glacial and checking asphalt layers on roads. Among the positive applicability of this method, in addition to its high resolution, are the speed of data collection as well as its non-invasive properties. In this way, data is collected in urban environments without having harmful effects on the environment.

The components of the GPR device are shown in Figure 7. The GPR device consists of a signal generator, a transmitter and a receiver. In addition to the display system, today's modern devices also have the ability to connect to Lab Top. Therefore, the basic processing of data during acquisition is also easily possible.

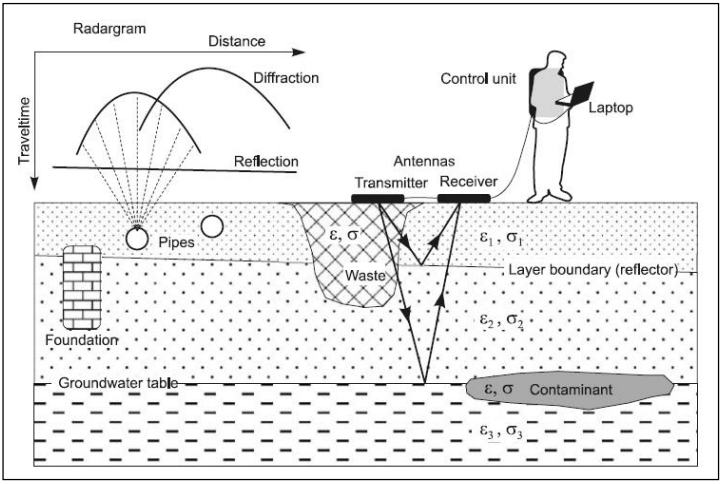

Figure 7: Schematic view of the principles of acquisition and components of the GPR.

GPR surveys are done both through continuous profiling and through surveying at fixed points. In continuous profiling, antennas are carried on the ground along the profile, and data are collected at specific spatial or temporal intervals. When a higher speed is needed for data acquisition, the antennas can be towed by a vehicle. When the electromagnetic pulse emitted from the transmitting antenna hits an electrical discontinuity, part of it passes through the interface and partly is reflected. This is caused by the change of impedance of electromagnetic waves at the interface of two environments. The amount of reflected and

transmitted energy as well as the amount of wasted energy (amortized) is a function of the electrical properties of the materials on both sides of the interface. To measure the round trip time of the electromagnetic wave that is transmitted from the transmitting antenna and returns to the receiving antenna after reflection from the subsurface targets, the depth of the desired target can be determined by the following equation.

$$D = \frac{Vt}{2}$$

D is the depth of the target, *t* is the corresponding time in the GPR time internal, and *V* is the speed of the GPR electromagnetic waves to the subsurface target. If the distance between the antennas is small compared to the depth of the target, this relationship accurately shows the depth of the subsurface target.

The speed of GPR waves in subsurface environments is calculated by the following equation.

$$V = \frac{C_0}{\sqrt{\varepsilon_r \mu_r \frac{1+\sqrt{1+(\sigma/\varepsilon\omega)}}{2}}}$$

C0 is the speed of the electromagnetic wave in the air, indicating the relative permeability of the magnetism and ε_r the relative transmissivity of the environment relative to the air, and ω is the angular frequency of the GPR pulse. The expression, $\sigma / \varepsilon\omega$

which is known as the loss factor, is close to zero in low-loss environments such as pure sand and can be ignored (Table 3). Also, the effect of μ_r in non-magnetic environments and in the range of GPR frequencies is small and it can be considered equal to 1 similar to non-magnetic environments. In this way, the following equation is summarized as follows.

$$V = \frac{C_0}{\sqrt{\varepsilon_r}}$$

In practice, the average speed of GPR waves in subsurface environments can be calculated by different ways. These methods include measuring the wave travel time from a buried target at a certain depth, direct laboratory measurements on field samples, measuring the wave travel time between boreholes using antennas inside the borehole. Measuring, tomography and Common Mid-Point (CMP) images. In some of the modern devices and software, the average speed of the subsurface medium is determined by determining the move out of diffraction hyperbolas. If none of the above methods can be used in an environment, the average speed can be dermined according to the type of subsurface environment.

If the conductivity of structures is low and in the absence of materials with high magnetic permeability, the reflection coefficient is expressed by the following equation. This equation shows the reflection coefficient with good accuracy in most geological conditions.

$$R = \frac{\sqrt{\varepsilon_{1r}} - \sqrt{\varepsilon_{2r}}}{\sqrt{\varepsilon_{1r}} + \sqrt{\varepsilon_{2r}}}$$

To provide a quantitative scale of the parameters discussed in this section, the electromagnetic characteristics of some geological structures are given in Table 3.

Table 3: Electromagnetic characteristics of a few materials

normal material	relative transmissivity (ε_r)	Conductivity (mS/M)	speed (M/nS)	Damping (dB/M)
air	1	0	0.30	0
distilled water	80	0.01	0.033	2×10^{-3}
fresh water	80	0.5	0.033	0.1
sea water	80	3×10^{3}	0.01	10^{3}
dry sand	3-5	0.01	0.15	0.01
saturated sand	20-30	0.1-1	0.06	0.03-0.3
limestone	4-8	0.5-2	0.12	0.4-1
shale	5-15	1-100	0.09	1-100
silt	5-30	1-100	0.07	1-100
clay	5-40	2-1000	0.06	1-300
granite	4-6	0.01-1	0.13	0.01-1
dry salt	5-6	0.01-1	0.13	0.01-1
ice	3-4	0.01	0.16	0.01

Chapter 3

Data measurement

3-1- Data collection

Geophysical studies were carried out to in detect the discontinuity of the subsurface deposits caused by tectonic activities in the Miankaleh area. Due to the dense vegetation of the area, the north-south routes leading from the sea coast to Gorgan Bay were selected in the satellite images, and at the end, 6 routes (profiles) with an approximate north-south trend were selected for magnetic measurements. The profiles are named in surveying order from number 1 to 6. Due to the availability and possibility of measuring resistivity data, additional measurements of resistivity and GPR were also carried out along profiles 1 to 3. The location of resistivity profiles is shown in Figure 8. In addition, the location of resistivity stations for all investigated profiles is given in Appendix A.

Magnetometry data collection in this study was done using two magnetometer devices. One of the devices was used as a base station to record the diurnal variation of the total magnetic field and to correct the measured data. Profiles were measured almost

perpendicular to the trend of the Miankaleh Peninsula, with an approximate north-south trend. In order to determine the position of the stations, GPS connected to the magnetometer device was used. Therefore, at the same time as the data is collected, the coordinates of the points are also collected to be used for drawing Magnetic profiles.

Data collection of electric resistivity was done simultaneously on profiles 1, 2 and 3. In addition, additional GPR and resistivity measurements with a minimum electrode spacing of 5 meters carried out in anomalous areas (observed in magnetometry profiles). In this study, the location of the stations was determined using a hand GPS, and all the required resistivity data were collected using dipole-dipole and pole-dipole arrays. The characteristics of the collected profiles, including their length, the number of points and station distances are given in Table 4.

Table 4: Characteristics of collected data in each profiles

Profile	Mag	Resistivity Phase 1	Array	Station spacing	GPR (m)	Resistivity Phase 2	Array	Station spacing
P1	372	487	DD	50/25 m	2840	983	DD	5 m
P2	307	174	PD; DD	50/25 m	1180	808	DD	5 m
P3	252	190	PD	50 m	1480	881	DD	5 m
P4	179	-	-	-	-	-	-	-
P5	202	-	-	-	-	-	-	-
P6	177	-	-	-	-	-	-	-
Data Sum	**1489**	**851**			**5500 m**	**2672**	**DD=Dipole-dipole; PD= Pole-dipole**	

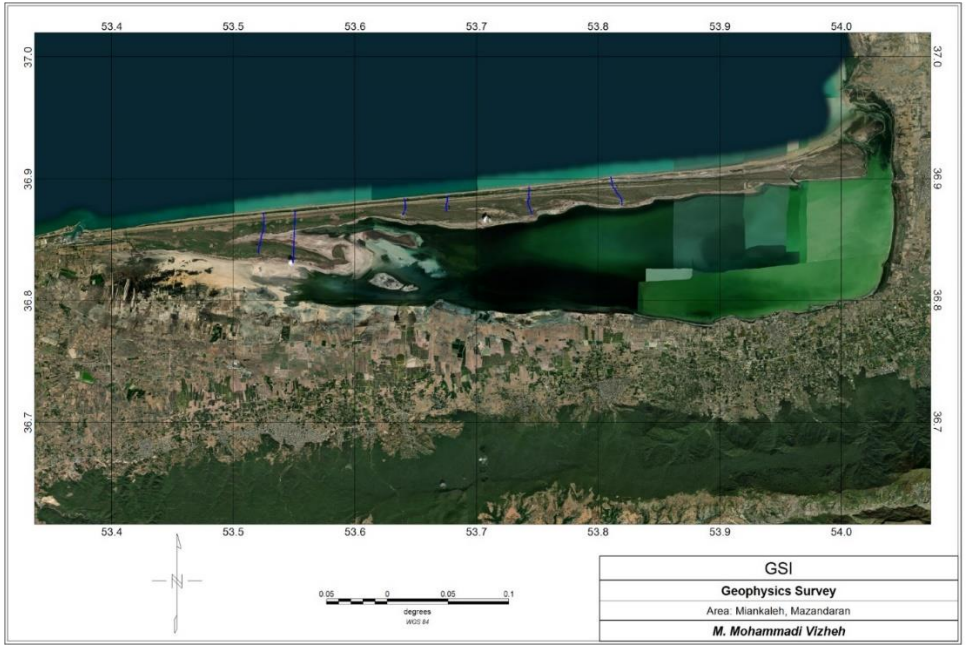

Figure 8: The position of the measured profiles (blue lines) on the satellite image (taken from the Global mapper software)

3-2- Data processing, modelling and data representation

One of the primary corrections is to remove outliers. In magnetometry survey, these readings are mainly related to the noise from metallic structures in the studied area and should be removed before the initial processing. Due to the location of most of the above mentioned profiles in the vicinity of urban environment and the location of power transmission lines, fences and buried gas pipelines, there was a limited number of outlier's data that were removed in the initial investigations. As mentioned, a magnetometer device was installed at the base station (Figure 9) during all the surveying days and recorded diurnal variation of the magnetic field regularly every 60 seconds, simultaneously with the measurements at the rover unit. The graph of magnetic field variation on 2022/06/24 is shown in Figure 10. Using the base station data, daily corrections have been done for all surveying days. After initial editing and daily corrections, magnetometry data have been levelled if needed.

Figure 9: Data measurement at the base station

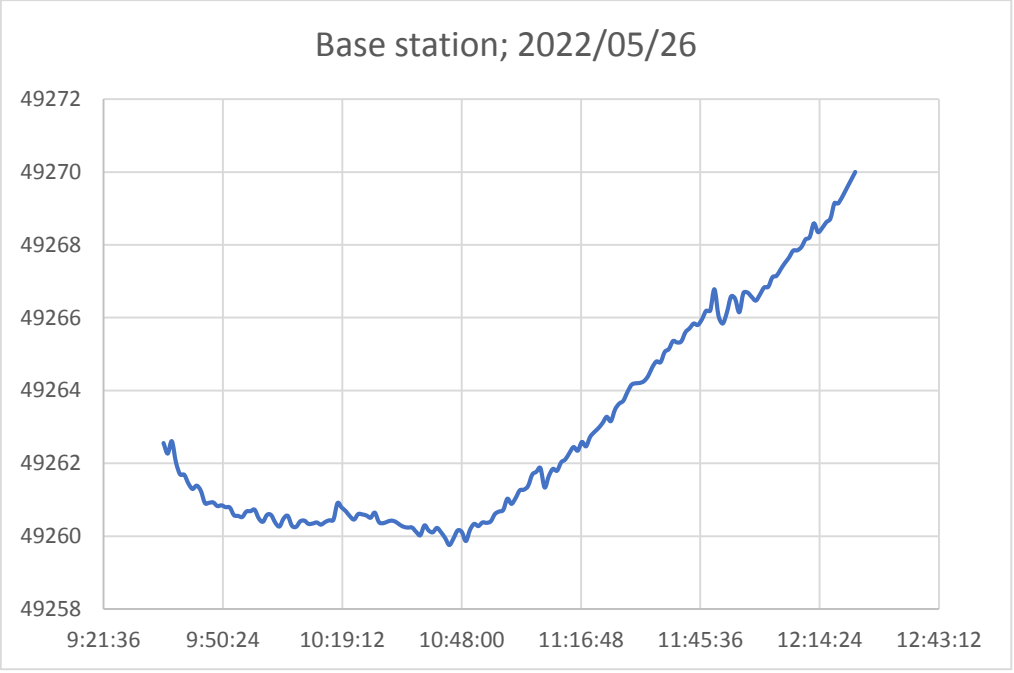

Figure 10: Variations in the intensity of the total magnetic field of the base station on 04/07/2013

One of the most common and advanced methods in geophysical data modeling is inversion, which is done with various methods and algorithms. In this type of modelling, the calculation process is obtained by starting from a simple model or using the results of geology data. Then, by changing the parameters of the model in each step of the inversion process, the difference between the response of the resulting model and the observed data is minimized. Since, generally, in geophysical studied, several models can be fitted to observed (measured) data, therefore, limitations such as the smoothness of the model are also considered during numerical calculations. In inversion, after determining the parameters of the model, all modelling steps are performed automatically. Res2Dinv, one of the most popular and well-known software, has been used for two-dimensional (2D) inversion of resistivity data in this study. Finally, Global mapper and Google earth software have been used for the joint interpretation of the result and the optimal representation of maps, models and sections.

It is worth mentioning that the used equipment's in this study are as follows (Figure 11 to Figure 19):

Figure 11: ARES device and related cables, with ELREC-10 reciever.

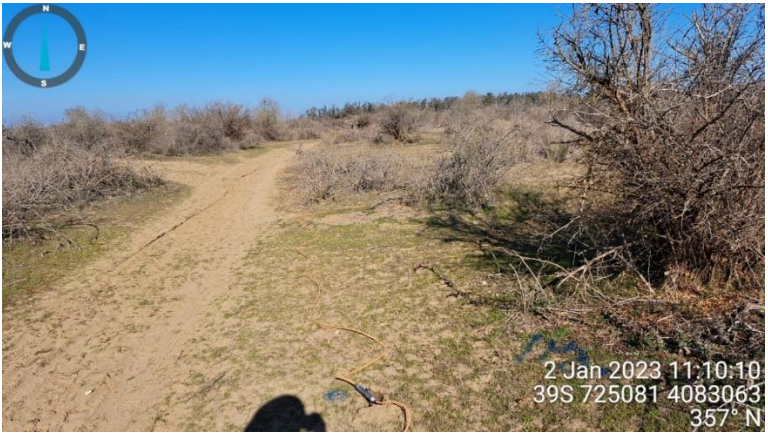

Figure 12: A view of resistivity surveying with ARES apparatus GEM.

Figure 13: A view magnetometer (GSM-19T model).

Figure 14: Magnetometric surveying.

Figure 15: GPR data surveying with 100 MHz unshielded antenna along profile 1.

Figure 16: GPR data surveying with 200 MHz unshielded antenna along profile 1.

Figure 17: CMP surveying for wave speed analysis using 100 MHz unshielded antenna at station 1330 along profile 2.

Figure 18: Control unit.

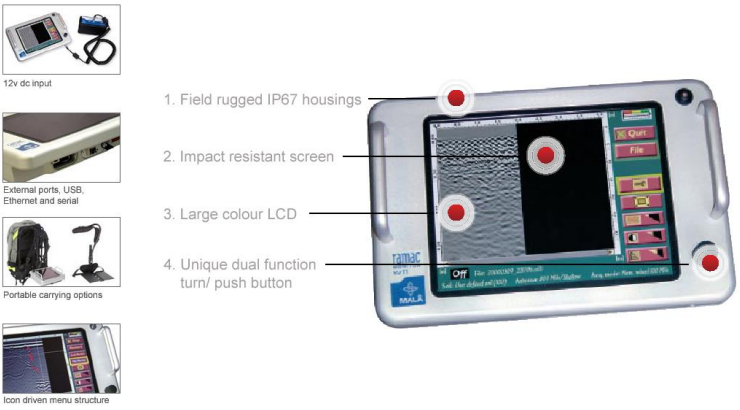

Figure 19: XV viewer and related equipment's.

Chapter 4

Results and Discussion

As mentioned earlier, to study and detect the discontinuities in the sedimentary deposits of the Miankaleh Peninsula, we used magnetometry, electrical resistivity and ground penetrating radar. Due to existing limitations, the location of investigated profiles is located in different places (Figure 8). Therefore, the name the profiles, selected in order of surveying. In the following, we will show the result of each profiles separately.

4-1- Profile 1

4-1-1- Magnetometry studies

Figure 8 shows the location of profile 1. The diagram of total magnetic intensity (TMI) variations along this profile is given in Appendix A. In most areas along the length of this profile, no significant changes observed in the TMI diagram. Figure 20 shows the variations in the TMI profile at station distances of 1400

to 1720 meters along profile 1. It should be noted that in this area the greatest changes in TMI profile have been recorded. The highest and lowest values of the TMI measured along profile 1 were 49257 and 49332 gammas, respectively, and the magnetic datum in this area is 49465 gammas. The difference between the highest and the lowest measured TMI is equal to 75 gammas.

As can be seen in Figure 20, the variation of the TMI is slightly greater than 30 gammas. Despite the slight variation in TMI profile, this difference is significant for homogeneous sedimentary deposits (coastal sands). These variations in magnetic properties are interpreted as different sedimentary units and their thickness changes on other sedimentary deposits and rock units (at relatively high depths). Changes in the TMI profile at the station distance of 1500 to 1550 meters (red bracket) are consistent with the slight change in the topography of the ground surface. This variation can be caused by the change in the thickness of the sand deposits due to the distortion of the underlying layers (due to the sedimentation process or tectonic activities), which will be assessed thoroughly in the resistivity data evaluation in the following subsection.

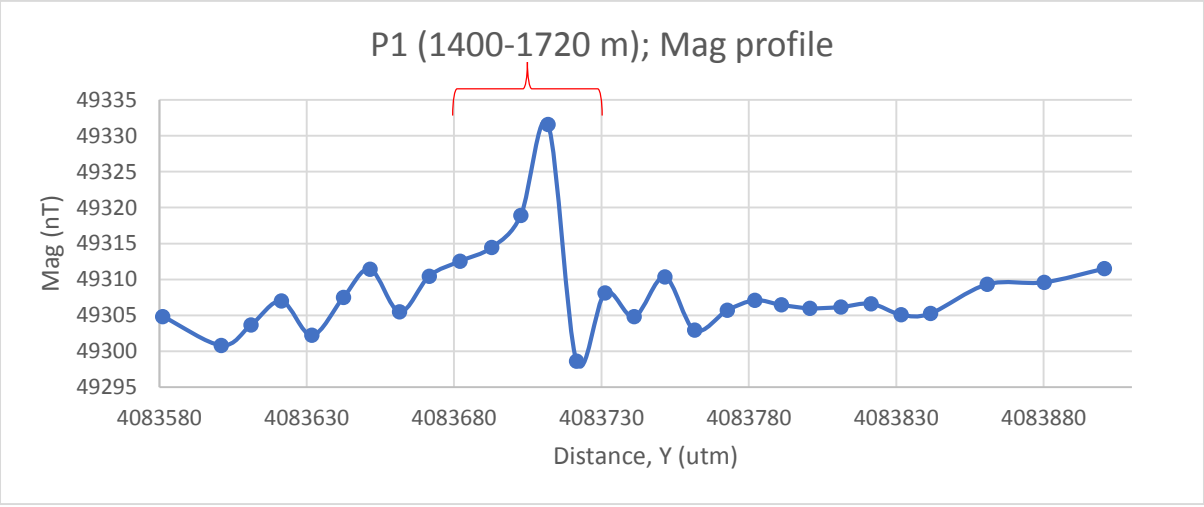

Figure 20: TMI profile at the station distance of 1400 to 1720 meters along profile 1, where relatively obvious changes in magnetic properties (red bracket) can be recognized at the specified distance. The horizontal axis shows the Y position of sampling stations in the UTM-WGS84 coordinate system.

4-1-2- Resistivity investigations

Figure 21 shows the model from the 2D inversion of resistivity data (with electrode spacing of 25 and 50 meters) by applying the topography of the earth's surface along profile 1. The minimum and maximum measured resistivity values (after removing outliers) along this profile are 0.03 and 396 Ωm, respectively. The mentioned values are the observed apparent resistivity and naturally, the values resulting from the inversion of the data will be different. It is worth noting that at the stations of 1570 to 1650 meters along the profile, resistivity data was measured in the range of 100 to 18000 Ωm. However, in order to perform the logical inversion process, the mentioned data has been removed before the data inversion. As can be seen in the inverted model (Figure 21), the range of resistivity changes along this profile is high. So that the maximum resistivity around station 1575 m exceeds 500 Ωm. This might be result of the location of boulders at shallow depths. In addition, the high water table and the presence of salt water in the sedimentary deposits is the result of resistivity decreasing in many areas. Several discontinuities can be recognized in the resistivity model, which can be result of fault activities in this area. These discontinuities are marked with black dashed lines in Figure 21. The position of the topography variation of the earth's surface and the sudden change in the magnetic

properties are indicated by red and black arrows in the inverted resistivity model, respectively. As can be seen, there is an acceptable correspondence between the topographical variations, the TMI profile and the resistivity data.

In order to investigate more details in the areas where obvious changes in magnetic properties and deep resistivity were observed, complementary resistivity measurements with a minimum electrode spacing of 5 meters were carried out using ARES device.

Figure 22 shows the model from the 2D inversion of resistivity data (with electrode spacing of 5 meters) by applying the topography of the earth's surface at the station spacing of 1405 to 1720 along profile 1. The minimum and maximum values of the measured resistivity data for this profile are 0.2 and 17698 Ωm, respectively. Similar to the 50 m electrode distance measurement (Figure 21), some data with high resistivity values in the station distance of 1570 to 1650 m were removed to make the data inversion process more favorable. As seen in the inverted model (Figure 21), the range of resistivity changes along this profile is also relatively high. The water table (white dashed line, WT) can be recognized at an altitude of -27 above sea level (a.s.l). This surface defines the boundary between dry and water-saturated sand deposits on both sides of the water table. The existence of the area with high

resistivity value in the distance between stations 1585 and 1590 m seems to be caused by the boulders that were used for improvement of road (due to the presence of sand dunes). However, several discontinuities can be detected in the resistivity model, which could be due to the fault activities in this area. These discontinuities are marked with black dashed lines in Figure 22. The position of the sudden changes in topography of the earth's surface and also TMI profile shown by red and black arrows in the inverted resistivity model, respectively. As can be seen, there is an acceptable correspondence between the topographical changes, the TMI profile and the inverted resistivity model.

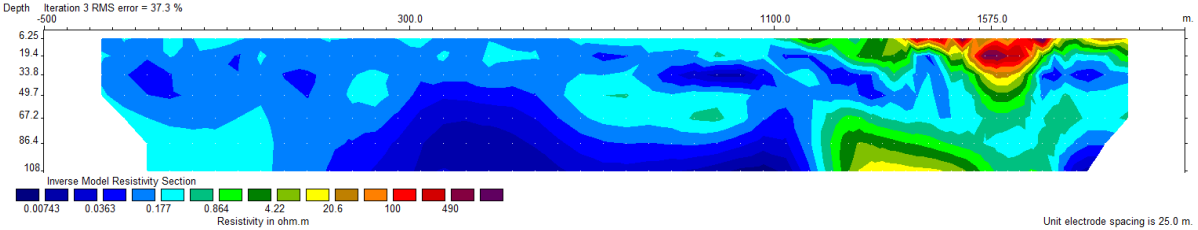

Figure 21: The model from the 2D inversion of resistivity data (stations spacing of 25 and 50 meters) along the profile 1. The position of significant changes in the magnetic properties and topography of the earth's surface are marked with black and red arrows, respectively.

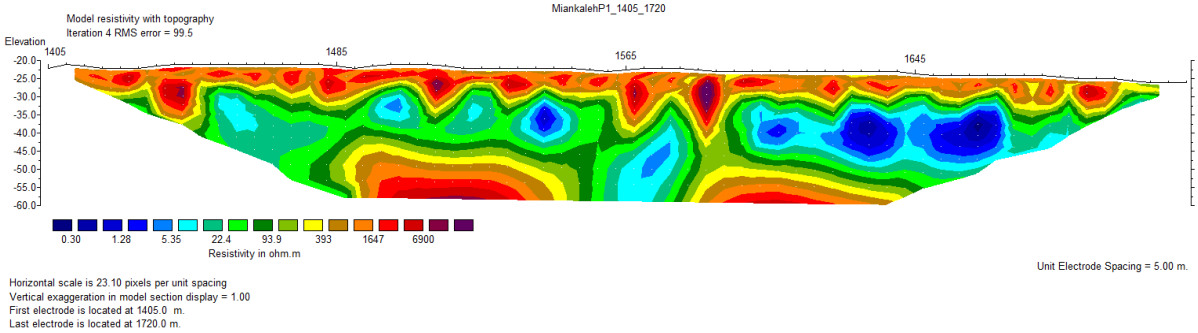

Figure 22: The model from the 2D inversion of resistivity data (station spacing of 5 meters) by applying the topography of the earth's surface along profile 1. The location of significant changes in the magnetic properties and topography of the earth's surface are specified with black and red arrows, respectively. The white dashed line is the water table (WT) and the black dashed lines are the subsurface discontinuities.

4-1-3 - GPR studies

In order to complete subsurface investigations in anomalous areas, GPR surveys were also carried out. Figure 23 & Figure 24 show the processed depth and time sections of GPR data using unshielded 100 and 250 MHz antennas at a station distance of 1400-1670 m, respectively. The relevant sections have been prepared after applying processes such as time zero correction, band-pass filtering, background removal, gain application, trace averaging, and topography correction. A velocity of 0.1 m/ns has been used time to depth conversion. As can be seen, at the place of the observed discontinuities in the magnetometry and resistivity data, deviations in the slope of the reflections of both sections are observed. The water table (WT) can be recognized as an almost horizontal reflection at the elevation of about -23 m a.s.l. Minor deviations in the continuity of the water table are caused by minor changes in the topography of the earth's surface, which is less than the accuracy of the used equipment (tape measure and handy GPS). It is necessary to explain that due to the low resistivity of the sedimentary deposits below the water table, reflections are not observed below this level. In addition, due to the transferability of sand deposits, the displacement of the reflection slope above the water table (blue arrows) can be caused by secondary fillings by sand deposits. However, the origin of these changes

can also be considered as a result of tectonic activities (due to the movement of subsurface faults) and before the sedimentation process. This case should be verified by trenching.

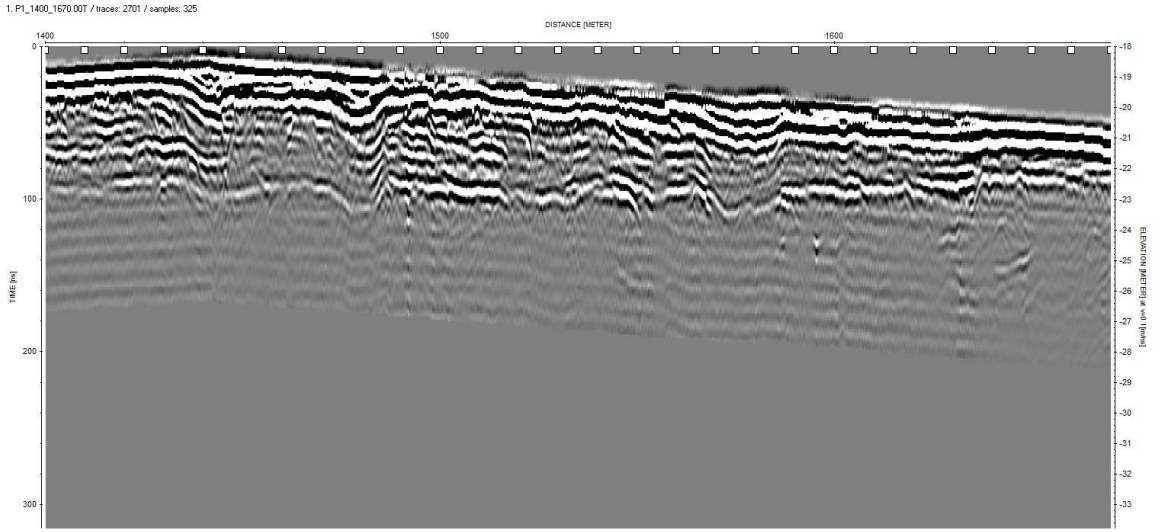

Figure 23: Time- and depth section (using an average velocity of 0.1 m/ns) processed by GPR using an unshielded 100 MHz antenna and applying topography correction at a station distance of 1400-1670 m along Profile 1. Location of significant changes in the TMI profile and topography of the earth's surface are indicated by black and red arrows, respectively. Secondary fills by sand deposits are marked with blue arrows.

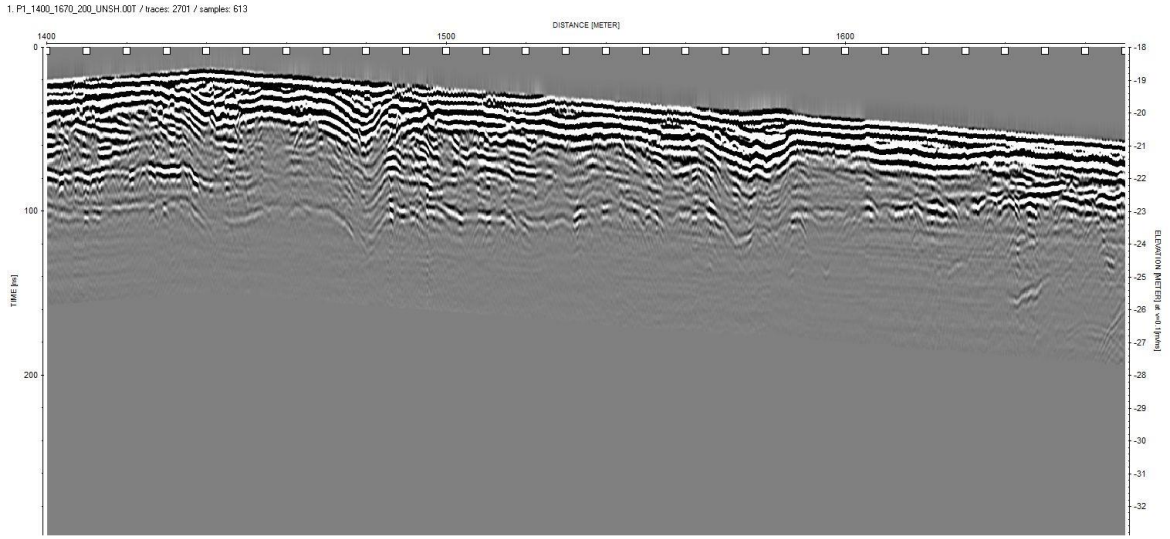

Figure 24: Time- and depth section (using average velocity of 0.1 m/ns) processed GPR using 100 MHz unshielded antenna and applying topography correction at station distance of 1400-1670 m along Profile 1. Location of significant changes in TMI profile and topography of the earth's surface are indicated by black and red arrows, respectively. Secondary fills by sands are marked with blue arrows.

4-2- Profile 2

4-2-1- Magnetometry studies

Figure 8 shows the location of profile 2. Similar to profile 1, no significant changes in the intensity of the magnetic field were observed in most areas along the length of the profile. The diagram of total magnetic field strength changes along this profile is given in Appendix A. Figure 25 shows the curve of changes in the intensity of the total magnetic field at a station distance of 1250 to 1525 meters along profile 2. It should be noted that in this area the greatest changes in magnetism intensity have been recorded. The highest and lowest values of the TMI measured along profile 2 were 49240 and 49296 gammas, respectively, and the background threshold in this area was considered to be 49465 gammas. The difference between the highest and the lowest measured TMI is equal to 56 gammas.

As can be seen in Figure 25, the variation of TMI is about 35 gammas. This rate of change is significant for homogeneous sedimentary deposits (coastal sands). Changes in magnetic properties are interpreted in relation to different sedimentary units and their thickness changes over other sedimentary deposits and rock units (at depth). The changes in magnetic intensity in the station distance of 1430 to 1525 meters of the profile

(red bracket) are consistent with the changes in the topography of the earth's surface. This phenomenon can be caused by the change in the thickness of the sand deposits due to the distortion of the underlying layers (due to the sedimentation process or tectonic activities).

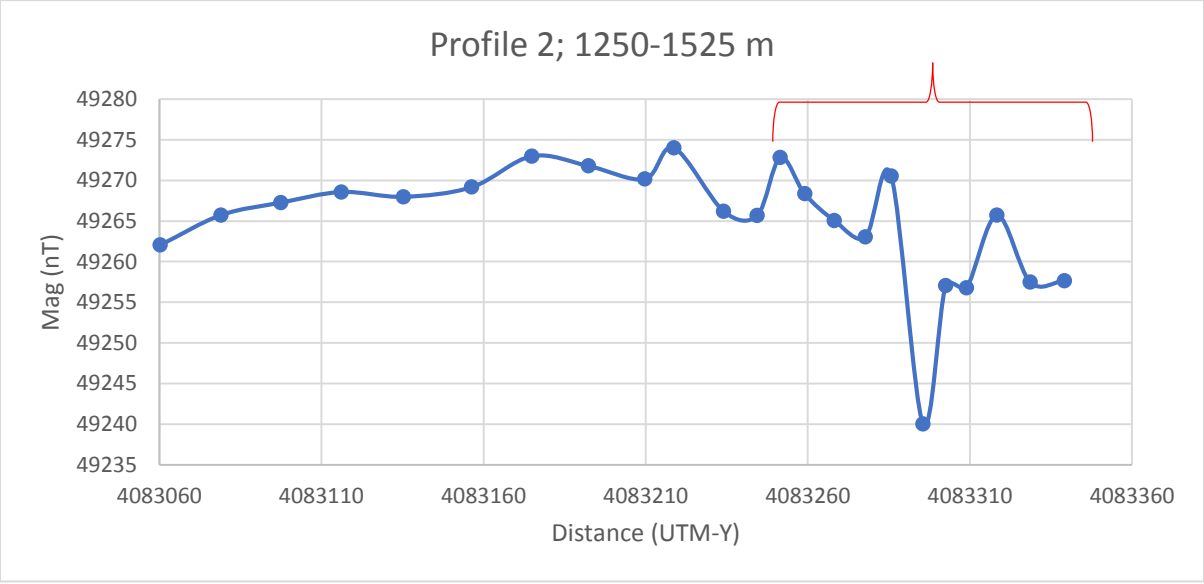

Figure 25: The diagram of the TMI at the station distance of 1250 to 1525 meters of profile 2, where relatively obvious changes in magnetic properties (red bracket) can be recognized at the resistivity. The horizontal axis shows the Y position of measured stations in the UTM-WGS84 coordinate system.

4-2-2- Resistivity studies

Figure 26 shows the model resulting from the 2D inversion of resistivity data (with electrode distance of 25 and 50 meters) by applying the topography of the earth's surface along profile 2. The minimum and maximum measured resistivity values (after removing outliers) along this profile are 0.1 and 135 Ωm, respectively. The mentioned values are the observed apparent resistivity and naturally, the values resulting from the inversion of the data will be different. It should be noted that unlike profile 1, resistivity data with a magnitude of 500 to 18,000 Ωm was not observed along this profile. However, in order to perform a logical inversion process, some outliers are removed before data inversion. As can be seen in the inverted model (Figure 26), the range of resistivity variations along this profile is not high, and the maximum resistivity near the surface and between the stations of 950 to 1300 meters exceeds 25 Ωm. These areas are interpreted in connection with the increase in the thickness of dry sands above the water table. Due to the large electrode distance (25 and 50 meters) compared to the depth of the water table (between 5 and 7 meters in high areas), the separation of dry sands has not been done well. The high water table and the presence of salt water in the sedimentary deposits cause a decrease in the resistivity in other places. Several discontinuities can be recognized in the

resistivity model, which can be caused by faults activity in this area. These discontinuities are marked with black dashed lines in Figure 26. The position of the change in the topography of the earth's surface and the sudden change in the magnetic properties are indicated by red and black arrows in the resistivity inversion model, respectively. As can be seen, there is an acceptable correspondence between the topographical changes, the intensity of the magnetic properties and the resistivity data.

In order to investigate more details in the areas where obvious changes in magnetic properties and deep resistivity were observed, additional resistivity measurements were made with ARES device and with a minimum electrode distance of 5 meters.

Figure 27 shows the model resulting from the 2D inversion of the resistivity data (with an electrode distance of 5 meters) by applying the topography of the earth's surface at the station distance of 1250 to 1525 along the profile 2. After removing the outlier data, the minimum and maximum measured resistivity values of this profile are 2.4 and 2909 Ωm, respectively. Similar to profile 1, some data with high resistivity (between 3000 and 80000 Ωm) were removed to make the data inversion process more favorable. As can be seen in the inverted model (Figure 27), the range of resistivity variations along this profile is also relatively high. The

water table (white dashed line) can be recognized at an altitude of -25 to compare with mean sea-level. This surface defines the boundary between dry and water-saturated sand deposits on both sides of the water table. Discontinuities in the resistivity model can be caused by the activity of faults and are marked by black dashed lines in Figure 27. The position of the change in the topography of the earth's surface and the sudden change in the magnetic properties are indicated by red and black arrows in the resistivity inversion model, respectively. As can be seen, there is an acceptable correspondence between the topographical changes, the intensity of the magnetic properties and the resistivity data.

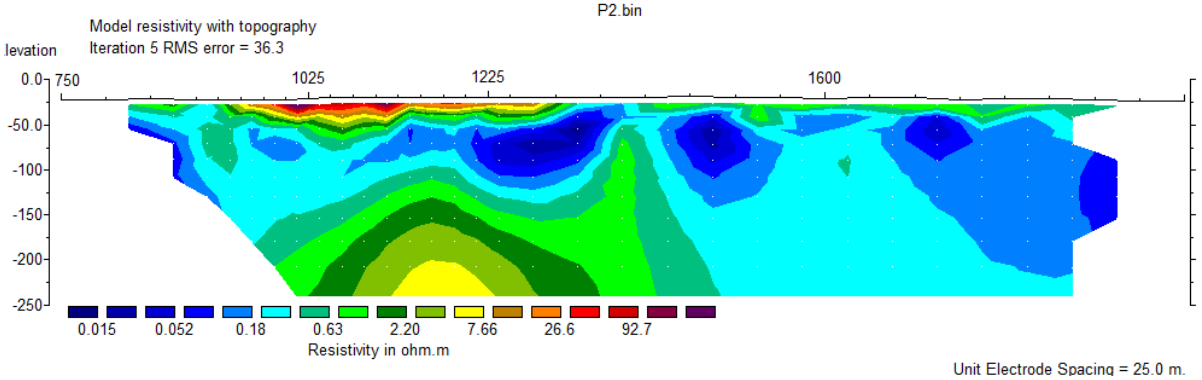

Figure 26: The model resulting from the 2D inversion of the resistivity data (electrode distance 25 and 50 meters) by applying the topography of the earth's surface along profile 2. The position of significant changes in the magnetic properties and topography of the earth's surface, are marked, with black and red arrows respectively.

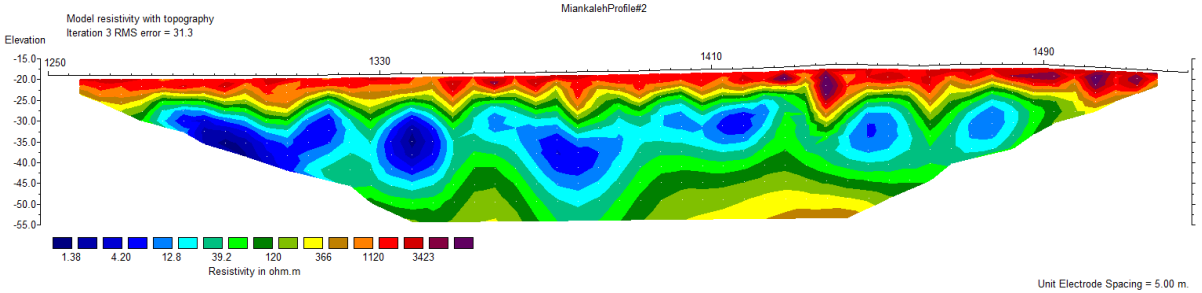

Figure 27: The model resulting from the 2D inversion of resistivity data (electrode distance 5 meters) by applying the topography of the earth's surface along profile 2. The location of significant changes in the magnetic properties and topography of the earth's surface are shown with black and red arrows, respectively. The white dashed line is the water table (WT) and the black dashed lines are the subsurface discontinuities.

4-2-3- GPR studies

Finally, in order to complete subsurface surveys in anomalous areas, GPR surveys were also carried out. In Figure 28 &Figure 29, the processed depth and time sections of GPR data using 100 and 250 MHz non-coverage antennas at a station distance of 1250 to 1490 meters are displayed respectively. Sections have been prepared after applying processes such as time-zero correction, band-pass filtering, background removal, gain application, trace averaging, and topography correction. A velocity of 0.1 m/ns has been used to convert time sections to depth. As can be seen, at the place of the observed discontinuities in the magnetometry and resistivity data, some can be detected deviations in the slope of the reflections of both sections. The water table (WT) can be recognized as an almost horizontal reflection at a height of about -22 meters above the mean sea-level. Minor deviations in the continuity of the water table are caused by minor changes in the topography of the earth's surface, which is less than the accuracy of the equipment used. It is necessary to explain that due to the low resistivity of the sedimentary deposits below the water table, reflections are not observed below this level. In addition, due to the transferability of sand deposits, the displacement of the reflection slope above the water table (blue arrows) can be caused by secondary fillings by sand deposits.

However, the source of these changes can also be considered as a result of tectonic activities (due to the movement of subsurface faults) and before the sedimentation process. This case should be verified by trenching.

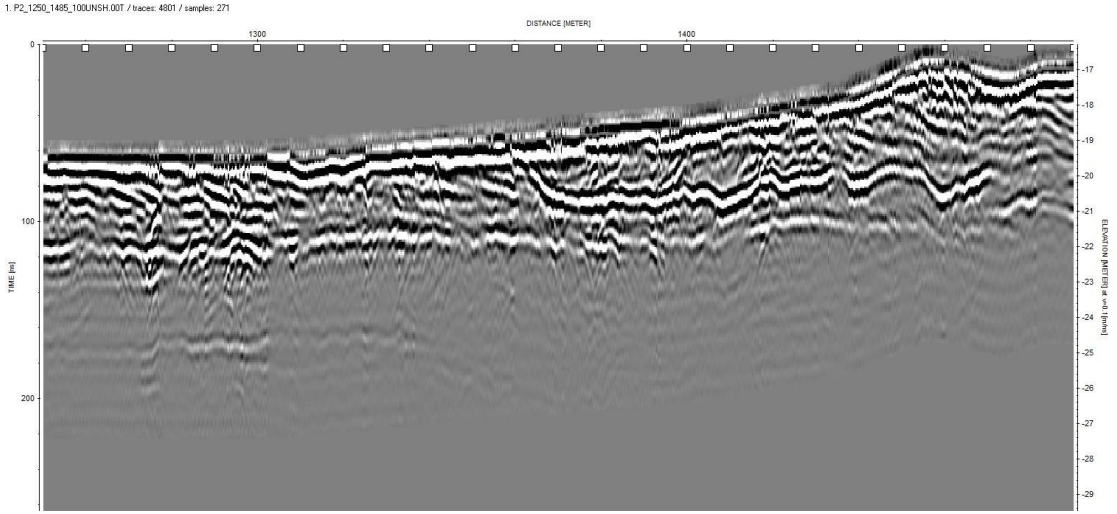

Figure 28: Time and depth section (using an average velocity of 0.1 m/ns) processed by GPR using an unshielded 100 MHz antenna and applying topography correction at the station distance of 1250 to 1490 in Profile 2. Significant changes in the magnetic properties and topography of the earth's surface are indicated by black and red arrows, respectively. Secondary fills by sand deposits are marked with blue arrows.

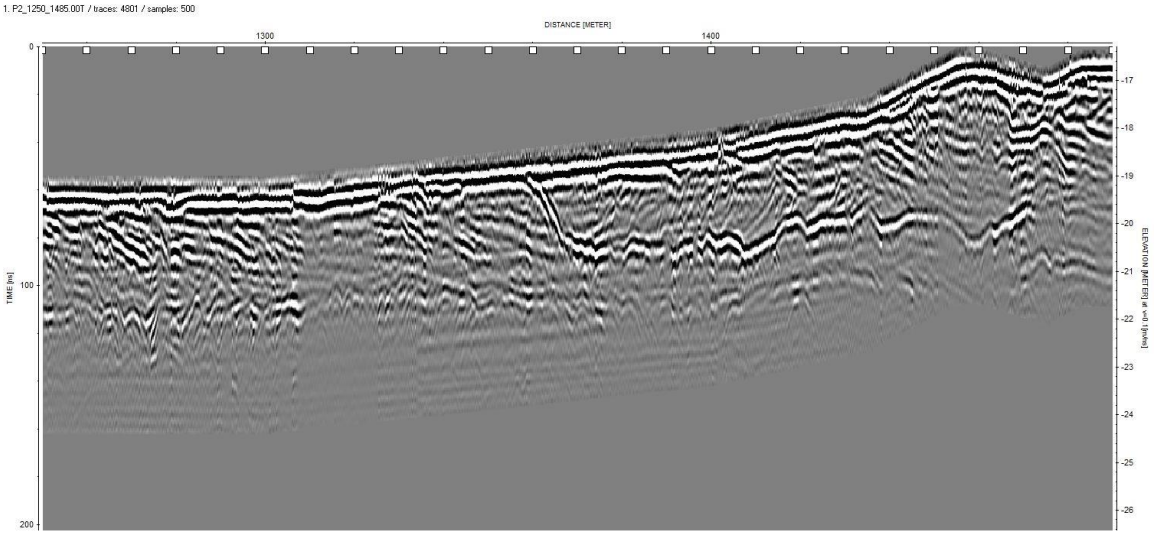

Figure 29: Time and depth section (using an average velocity of 0.1 m/ns) processed by GPR using a unshielded 200 MHz antenna and applying topography correction at the station distance of 1250 to 1490 Profile 2. Significant changes in The magnetic properties and topography of the earth's surface are indicated by black and red arrows, respectively. Secondary fills by sand deposits are marked with blue arrows.

4-3- Profile 3

4-3-1- Magnetometry studies

Figure 8 shows the location of profile 3. No significant changes in the intensity of the magnetic field were observed along this profile. The diagram of total magnetic field strength changes along this profile is given in Appendix A. Figure 32 shows the curve of variation in the intensity of the total magnetic field at the station distance of 1100 to 1415 meters in profile 3. Similar to the previous profiles, the greatest changes in the intensity of magnetism have been recorded in this area. The maximum and lowest values of the TMI measured along profile 3 were 49291 and 49359 gammas, respectively, and the background limit in this area was considered to be 49465 gammas. The difference between the maximum and the minimum measured TMI is equal to 68 gammas.

As can be seen in Figure 30, the variation of the magnetic field intensity is slightly less than 20 gammas. This rate of change is significant for homogeneous sedimentary deposits (coastal sands). Changes in magnetic properties are interpreted due to the different sedimentary units and their thickness variations at depth. Variations in the intensity of magnetism at the station distance of 1130 to 1230 meters along the profile (red

bracket) are consistent with the slight change in the topography of the earth's surface. Similar to the previous profiles, these variations can be caused by the change in the thickness of the sand deposits due to the distortion of the underlying layers (due to the sedimentation process or tectonic activities). This case will be evaluated in the review of resistivity data.

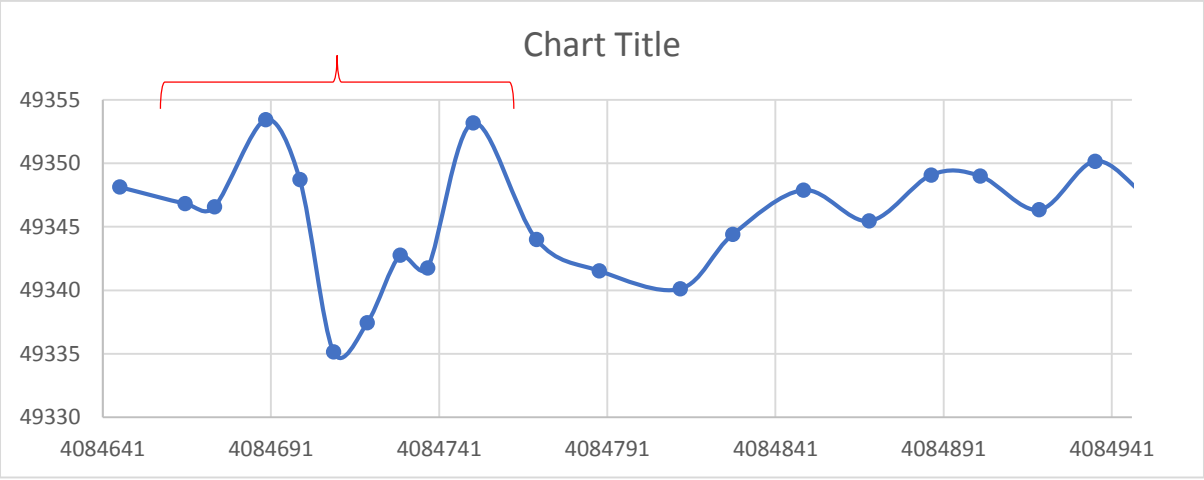

Figure 30: The diagram of the total intensity of the magnetic field at the station distance of 1100 to 1415 meters of profile 3, where relatively obvious changes in magnetic properties (red bracket) can be recognized at the specified distance. The horizontal axis shows the Y position of measured stations in the UTM-WGS84 coordinate system.

4-3-2- Resistivity studies

Figure 31 shows the model resulting from the 2D inversion of resistivity data (with electrode distance of 25 and 50 meters) by applying the topography of the earth's surface along profile 1. The minimum and maximum measured resistivity values (after removing outliers) along this profile are 0.17 and 5.1 Ωm, respectively. The mentioned values are the observed apparent resistivity and naturally, the values resulting from the inversion of the data will be different. It should be noted that, similar to the previous profiles, a number of outlier resistivity data between 30 and 660 Ωm were measured. However, in order to perform the logical inversion process, these data have been removed before the data inversion. As can be seen in the inverted model (Figure 31), the range of resistivity changes along this profile is very small. Due to the large electrode distance (25 and 50 meters) compared to the depth of the water table (between 4 and 6 meters in high areas), the separation of dry sands has not been done well. The high water table and the presence of salt water in the sedimentary deposits cause a decrease in the resistivity in other places. Several discontinuities can be recognized in the resistivity model, which might be the result of fault activities in this area. These discontinuities are marked with black dashed lines in Figure 31. The position of the change in the topography of the earth's

surface and the sudden change in the magnetic properties are indicated by red and black arrows in the resistivity inversion model, respectively. As can be seen, there is an acceptable correspondence between the topographical changes, the intensity of the magnetic properties and the resistivity data.

In order to investigate more detail studies in the areas where obvious changes in magnetic properties and deep resistivity were observed, additional measurements of resistivity were made with ARES device and with a minimum electrode distance of 5 meters.

Figure 32 shows the model resulting from the 2D inversion of the resistivity data (with an electrode distance of 5 meters) by applying the topography of the earth's surface at the station distance of 1100 to 1415 along profile 1. The minimum and maximum measured resistivity values of this profile are 0.74 and 3876 Ωm, respectively. The mentioned values are the observed apparent resistivity and naturally, the values resulting from the inversion of the data will be different. In this profile, some data with very low and high resistivity were removed so that the process of data inversion can be done in a more favorable way. As seen in the inverted model (Figure 32), the range of resistivity changes along this profile is also high. The water table (white dashed line) can be recognized at an altitude of -25 above mean sea-level. This surface defines the boundary between dry

and water-saturated sand deposits on both sides of the water table. In addition, several discontinuities can be detected in the resistivity model, which can be caused by the fault activities in this area. These discontinuities are marked with black dashed lines in Figure 32. The position of the change in the topography of the earth's surface and the sudden change in the magnetic properties are indicated by red and black arrows in the resistivity inversion model, respectively. As can be seen, there is an acceptable correspondence between the topographical changes, the intensity of the magnetic properties and the resistivity data.

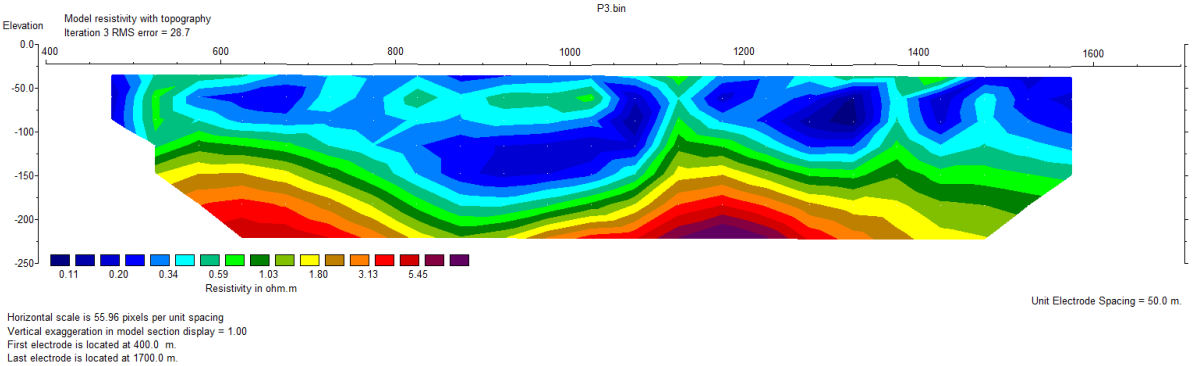

Figure 31: The model resulting from the 2D inversion of the resistivity data (electrode distance 50 meters) by applying the topography of the earth's surface along profile 3. The location of significant changes in the magnetic properties and topography of the earth's surface are specified with black and red arrows, respectively.

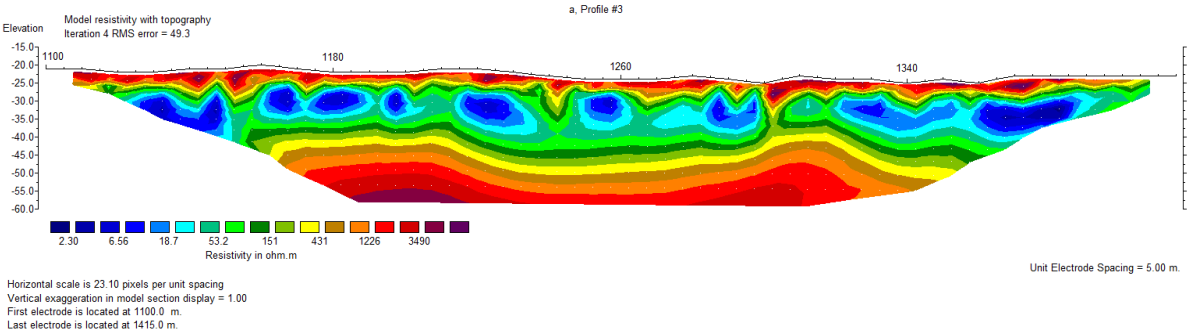

Figure 32: The model resulting from the 2D inversion of resistivity data (electrode distance 5 meters) by applying the topography of the earth's surface along profile 3. The location of significant changes in the magnetic properties and topography of the earth's surface are specified with black and red arrows, respectively. The white dashed line is the water table (WT) and the black dashed lines are the subsurface discontinuities.

4-3-3- GPR studies

In order to complete subsurface surveys in anomalous areas, GPR surveying were also carried out. Figure 33 shows the depth and time processed section of GPR data using non-coverage 250 MHz antenna at the station distance of 1100 meters to 1390 meters. This section has been prepared after applying processes such as time-zero correction, band-pass filtering, background value removal, gain application, trace averaging, and topography correction. A velocity of 0.1 m/ns has been used to convert time sections to depth. As can be seen, in places of discontinuities in the magnetometry and resistivity data, deviations in the slope of the reflections can be recognized. The water table can be recognized as a reflection (WT) at a height of about -23 meters above the mean sea-level. The reason for the significant deviations and also the change in the height of the water table is due to the significant changes in the topography of the earth's surface, which was less than the accuracy of the used equipment’s (meters and handy GPS). It is worth noting that due to the low resistivity of the sedimentary deposits below the water table, reflections are not observed below this level. In addition, due to the transferability of sand deposits, the displacement of the reflection slope above the water table (blue arrows) can be caused by secondary fillings by sand deposits. However, the origin of these changes can also be

considered as a result of tectonic activities (due to the movement of subsurface faults) and before the sedimentation process. This issue should be verified by trenching.

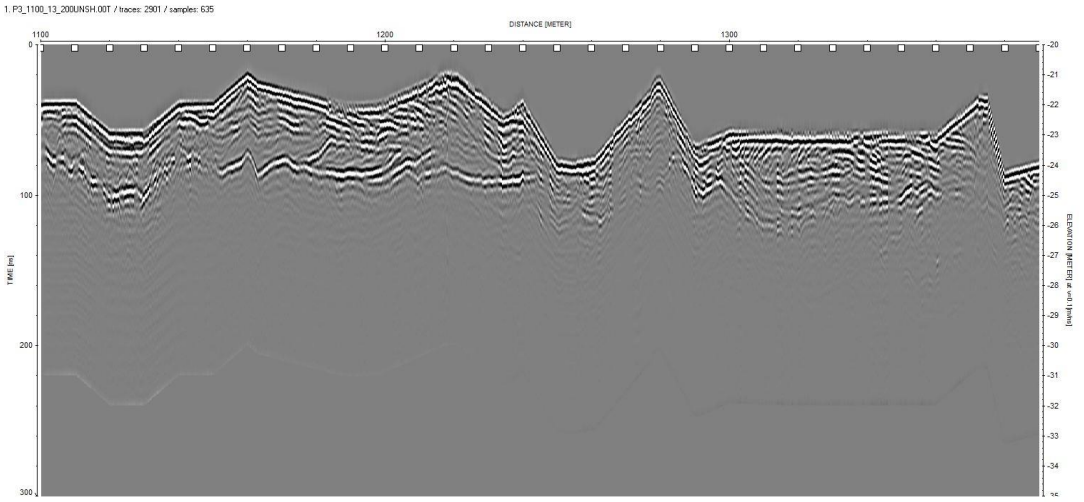

Figure 33: Time and depth section (using an average velocity of 0.1 m/ns) processed by GPR using a unshielded 200 MHz antenna and applying the approximate topography of the earth's surface at a station distance of 1100 to 1390 in Profile 3. Position of notable changes of the magnetic properties and topography of the earth's surface are marked with black and red arrows, respectively. Secondary fills by sand deposits are marked with blue arrows.

4-4- Profile 4

4-4-1- Magnetometry studies

Figure 8 shows the location of profile 4. Figure 34 shows the curve of variations in the intensity of the total magnetic field along profile 4. The maximum and minimum values of the TMI measured along this profile are 49327 and 49363 gammas, respectively, and the background threshold in this area was considered to be 49465 gammas. The difference between the maximum and minimum intensity of the measured total magnetic field is equal to 36 gammas. The collected data in the vicinity of metal structures (huts, boats, fences, etc.) have been removed and can be recognized such as discontinuities in the diagram.

As can be seen in Figure 34, the variations of the magnetic field intensity are slightly greater than 30 gammas. Majority of these variations are caused by the gradual and regional increase of the magnetic field towards the north. However, local changes can be detected at different points, the most important of which are the changes around 4085000 latitudes. Variations in magnetic properties are interpreted in relation to different sedimentary units and their thickness variations on other sedimentary deposits and rock units (at relatively high depths). The changes in magnetic

intensity at the latitude of 4085000 (red bracket) are consistent with the minor changes in the topography of the earth's surface. Similar to the previous profiles, this issue is interpreted in relation to the change in the thickness of the sand deposits caused by the distortion of the underlying layers (due to the sedimentation process or tectonic activities).

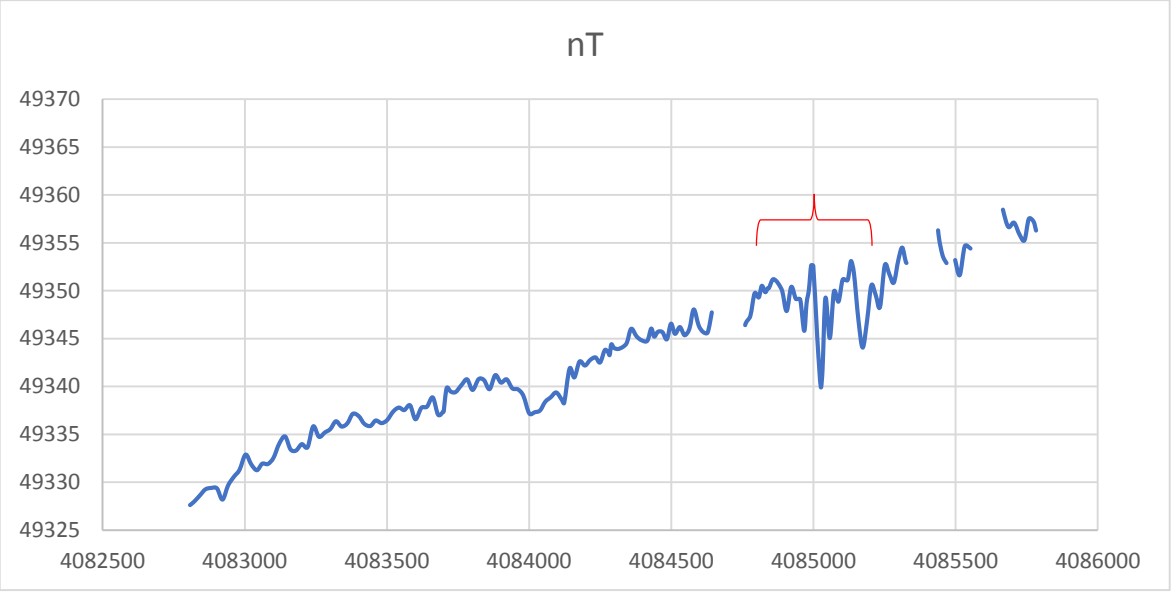

Figure 34: The diagram of the total intensity of the magnetic field along profile 4, where relatively obvious changes in magnetic properties are shown with red bracket. The horizontal axis shows the Y position of measured stations in the UTM-WGS84 coordinate system.

4-5- Profile 5

4-5-1- Magnetometry studies

Figure 8 shows the location of profile 5. Figure 35 shows the curve of changes in the intensity of the total magnetic field along profile 5. The maximum and minimum values of the TMI measured along this profile are 49347 and 49380 gammas, respectively, and the background threshold in this area was considered to be 49465 gammas. The difference between the maximum and minimum intensity of the measured total magnetic field is equal to 33 gammas. The collected data in the vicinity of metal structures (huts, boats, fences, etc.) have been removed and can be recognized as discontinuities in the diagram.

As can be seen in Figure 35, the variation of the magnetic field intensity is slightly greater than 30 gammas. Majority of these changes are caused by the gradual and regional increase of the magnetic field towards the north. However, local changes can be detected at different points, the most important of which are the changes around 4085800 latitudes. Changes in magnetic properties are interpreted in relation to different sedimentary units and their thickness variations on other sedimentary deposits and rock units (at relatively high depths). The changes in magnetic

intensity at the latitude of 4085800 (red bracket) are consistent with the minor changes in the topography of the earth's surface. Similar to the previous profiles, this phenomenon is interpreted in relation to the change in the thickness of the sand deposits caused by the distortion of the underlying layers (due to the sedimentation process or tectonic activities).

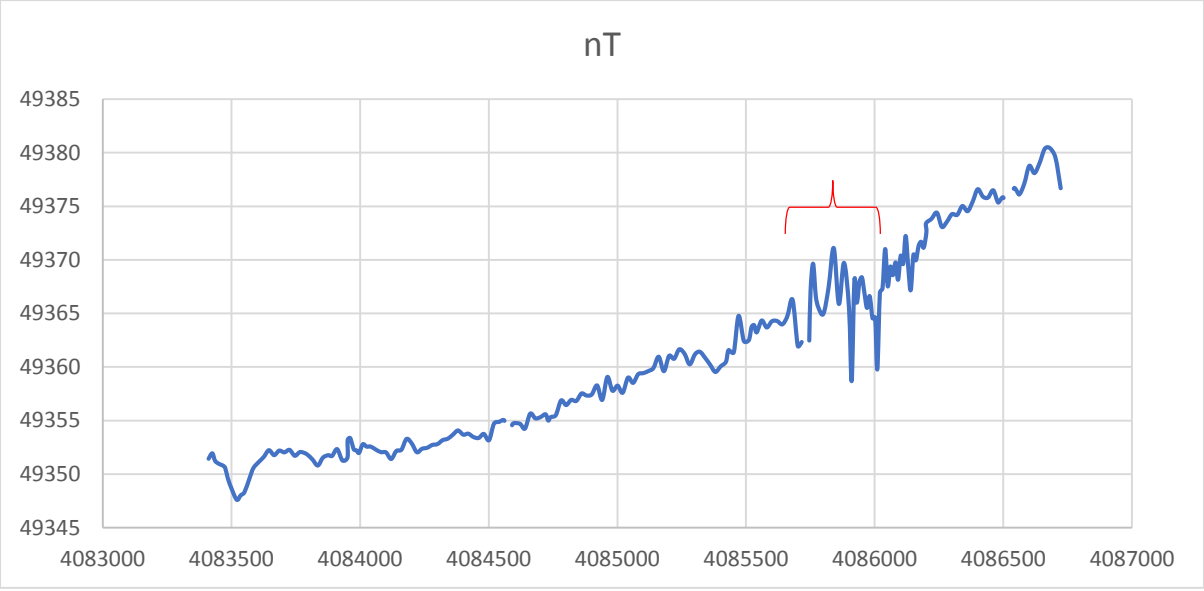

Figure 35: The diagram of TMI along profile 5, where relatively obvious changes in magnetic properties are shown with red bracket. The horizontal axis shows the Y position of measured stations in the UTM-WGS84 coordinate system.

4-6- Profile 6

4-6-1 Magnetometry studies

Figure 8 shows the location of profile 6. Figure 36 shows the curve of changes in the intensity of the total magnetic field along profile 6. The highest and lowest values of the TMI measured along this profile are 49378 and 49429 gammas, respectively, and the background threshold in this area was considered to be 49465 gammas. The difference between the maximum and minimum intensity of the measured total magnetic field is equal to 51 gammas. The collected data in the vicinity of metal structures (huts, boats, fences, etc.) have been removed and can be recognized as discontinuities in the diagram.

As can be seen in Figure 36, the variation of the magnetic field intensity is slightly greater than 50 gammas. Majority of these changes are caused by the gradual and regional increase of the magnetic field towards the north. However, local changes can be detected at different points, especially around 4087300 latitudes. Variation in magnetic properties are interpreted in relation to different sedimentary units and their thickness changes on other sedimentary deposits and rock units (at relatively high depths). The changes in magnetic intensity at the latitude of 4087300 (red

bracket) are consistent with the minor changes in the topography of the earth's surface. Similar to the previous profiles, this phenomenon is interpreted in relation to the change in the thickness of the sand deposits caused by the distortion of the underlying layers (due to the sedimentation process or tectonic activities).

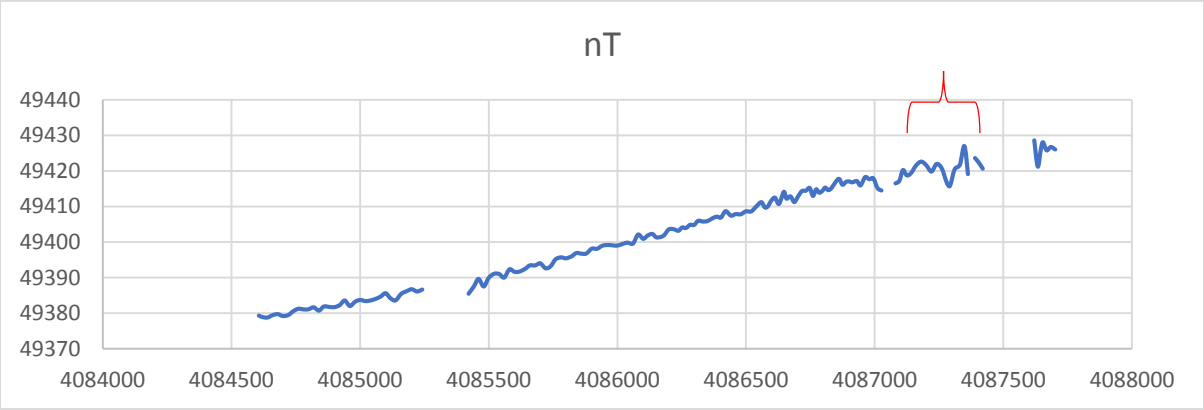

Figure 36: The diagram of the total intensity of the magnetic field along profile 6, where relatively obvious changes in magnetic properties are shown with red bracket. The horizontal axis shows the Y position of measured stations in the UTM-WGS84 coordinate system.

Chapter 5

Conclusion and Recommendations

Geophysical studies were carried out in order to investigate features resulted due to the tectonic activities, and to detect the buried faults in recent sediments in the protected Miankaleh Peninsula. In this regard, 6 profiles were designed to collect resistivity, magnetometry and GPR data in this area. Due to the dense vegetation of the studied area, the profiles selected in a N-S trend along the available traffic path. Considering the existing limitations, it was possible to implement all the mentioned geophysical methods only in three profiles (Profiles 1, 2 and 3) and the remaining ones (Profiles 4, 5 and 6) were evaluated only by magnetometry method.

The results of magnetometry studies show relatively low variations in TMI profiles along the measured profiles. Apart from the anomalous areas along the profiles, it seems that in the other part of the studied areas, the sedimentary deposits (mainly sand and silt) have significant thickness. Low variations in the TMI profiles can be considered as a result of this phenomenon. It should be noted that sudden changes of about 10 to 30 gammas can be seen on sand dunes or in their vicinity. At first glance, the topographical changes of the earth's surface (caused by wind and coastal sand

deposits) seem to be the main factor of these changes. Although, these changes can also be seen in some areas in the flat parts of the sand dunes.

In the 1st phase of the survey, magnetometry and resistivity studies (electrode spacing of 50 and 25 m), abnormal areas were revealed mainly around sand dunes. Therefore, resistivity studies with higher resolution (electrode spacing of 5 m) and GPR surveys were also carried out in abnormal areas of Profiles 1, 2 and 3. The results of resistivity studies show relatively large resistivity variations in the studied areas. The main cause of this phenomenon is the presence of dry sand deposits above the water table, water salinity below the water table, and the presence of rock structures at depth. In some areas, the increase in the thickness of the sand deposits can be well recognized from the models on 2D inversion of resistivity data. The resistivity data, which can be considered caused by fault activity, can be seen in Profiles 1 and 2. It should be noted that minor discontinuities were observed in all inverted resistivity models. Below the water table, due to the low resistivity of sedimentary deposits (sand and silt saturated with salt water) and the type of the used inversion (i.e. smoothness constrains), it is difficult to detect discontinuities in resistivity models. However, GPR measurements have revealed significant distortions in the sedimentary interfaces beneath the dunes. The mentioned distortions under the sand dunes show an acceptable

correlation with variations in the TMI profiles and sometimes confirm the discontinuities in the resistivity models. Figure 37 to Figure 39 show the results of geophysical studies in the abnormal areas of Profiles 1 to 3, respectively. In order to evaluate and verify the results of geophysical studies, at this stage, 4 exploration trenches are proposed at the anomalous areas along these profiles. The coordinates of the center of the proposed trenches are given in Table 5, with an approximate north-south trend (along the measured profiles). To implement the proposed trenches, the azimuth of 0 to 10 degrees relative to the north is considered in order to minimize environmental damage.

Table 5: The position of the center of the proposed trenches in the UTM_WGS84 coordinate system

Profile	Station	UTM zone	X	Y	Azimuth (°)	Priority
P2	P2_1420	39S	725051	4083240	0-10	1
P2	P2_1475	39S	725017	4083295	0-10	2
P3	P3_1200	39S	735395	4084739	0-10	3
P1	P1_1530	39S	727328	4083708	0-10	4

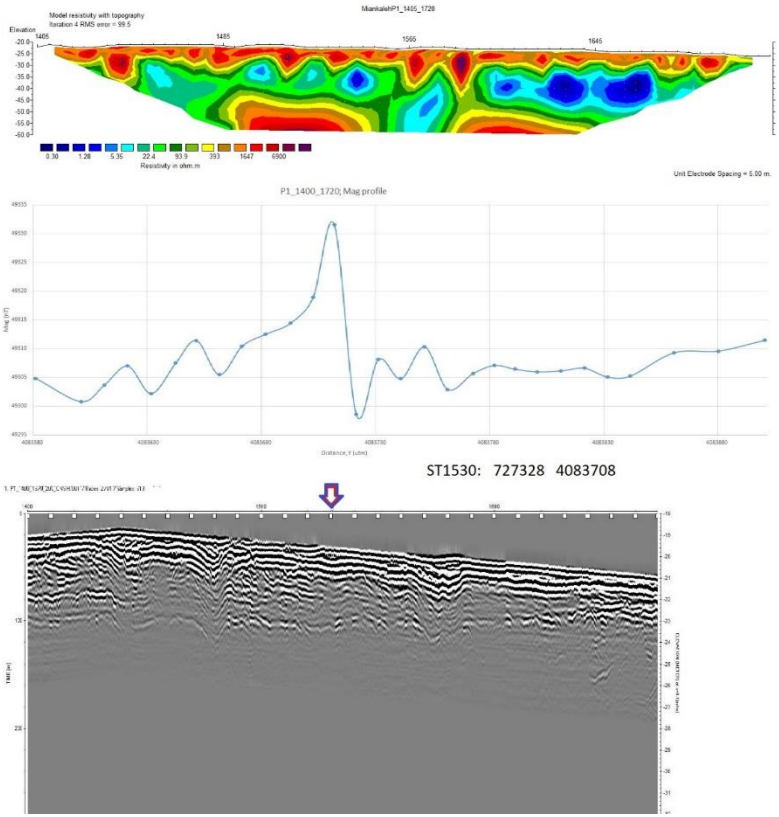

Figure 37: Joint interpretation of the results along the anomalous areas of Profile 1: the model from 2D inversion of the resistivity data (top), the TMI profile (middle) and the processed time- and depth section of the GPR data using an unshielded 200 MHz antenna. The colored arrow is the position of the center of the proposed trench.

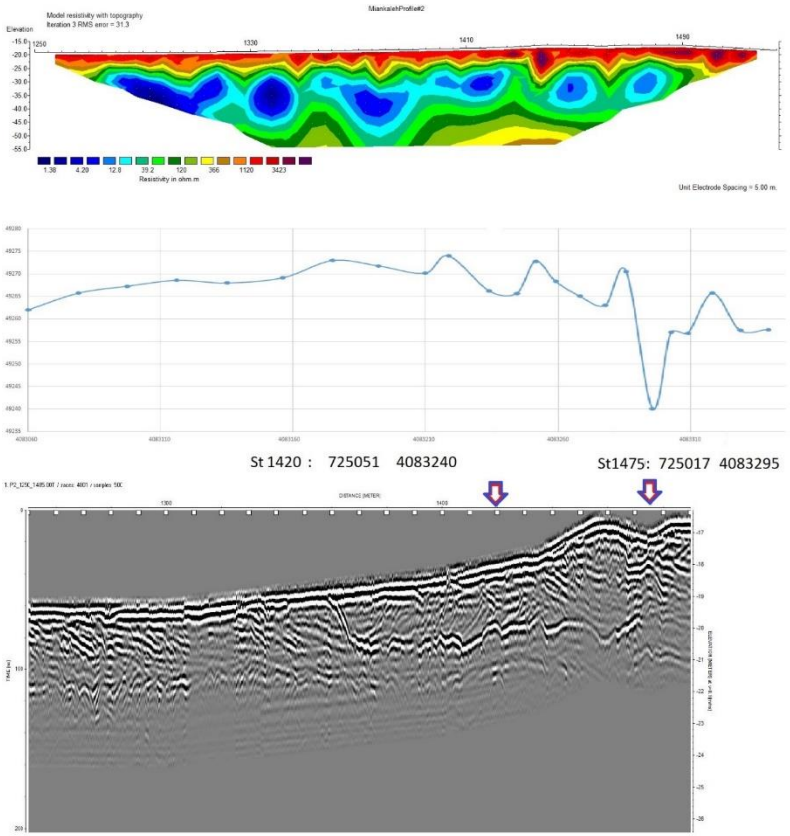

Figure 38: Joint interpretation of the results along the anomalous areas of Profile 2: the model from 2D inversion of the resistivity data (top), the TMI profile (middle) and the processed time- and depth section of the GPR data using an unshielded 200 MHz antenna. The colored arrow is the position of the center of the proposed trench.

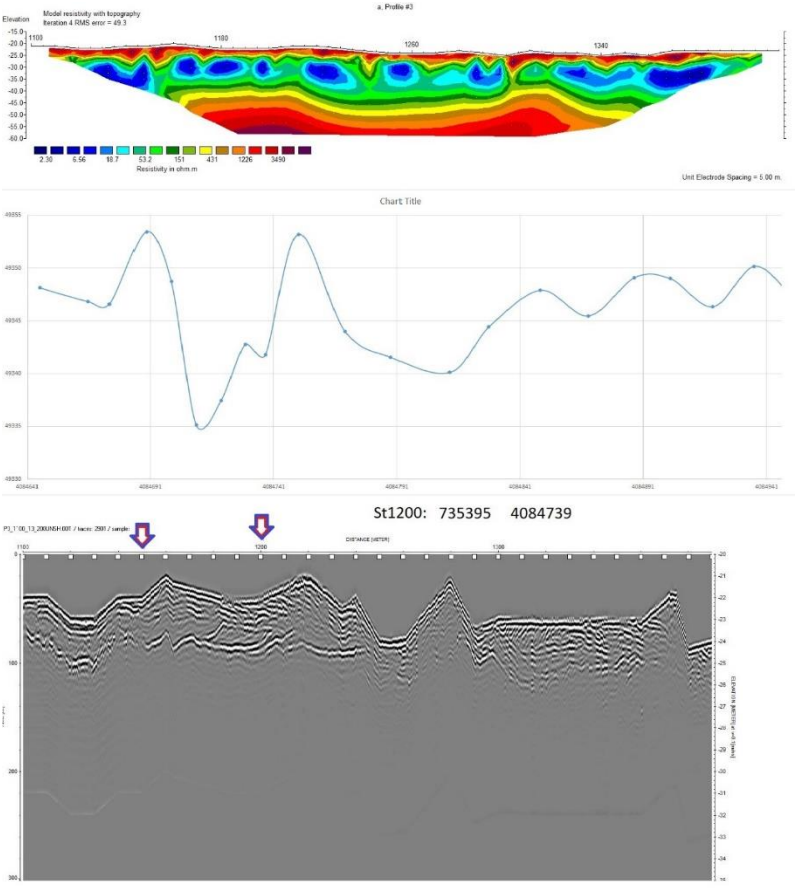

Figure 39: Joint interpretation of the results along the anomalous areas of Profile 3: the model from 2D inversion of the resistivity data (top), the TMI profile (middle) and the processed time- and depth section of the GPR data using an unshielded 200 MHz antenna. The colored arrow is the position of the center of the proposed trench.

APPENDIX

APPENDIX A: Position of resistivity stations (Profiles 1,2 and 3)

Station	X	Y	Z
P1 -500	727299	4081685	-21
P1 -450	727299	4081735	-20
P1 -400	727297	4081784	-20
P1 -350	727303	4081834	-20
P1 -300	727303	4081882	-20
P1 -250	727305	4081934	-21
P1 -200	727307	4081984	-22
P1 -150	727308	4082034	-22
P1 -100	727311	4082084	-22
P1 -50	727312	4082134	-21
P1 -0	727310	4082183	-20
P1 -50	727305	4082233	-19
P1 -100	727309	4082282	-19

P1 -150	727308	4082334	-19
P1 -200	727313	4082382	-19
P1 -250	727311	4082432	-20
P1 -300	727309	4082482	-19
P1 -350	727305	4082532	-19
P1 -400	727302	4082582	-19
P1 -450	727306	4082632	-19
P1 -500	727310	4082682	-20
P1 -550	727314	4082732	-21
P1 -600	727321	4082781	-21
P1 -650	727323	4082831	-20
P1 -700	727315	4082881	-21
P1 -750	727321	4082930	-21
P1 -800	727318	4082980	-20
P1 -850	727318	4083030	-20
P1 -900	727318	4083080	-20
P1 -950	727319	4083130	-19
P1 -1000	727312	4083181	-19

P1 -1050	727314	4083230	-19
P1 -1100	727316	4083279	-19
P1 -1150	727318	4083328	-20
P1 -1200	727316	4083380	-20
P1 -1250	727317	4083430	-21
P1 -1300	727318	4083480	-21
P1 -1350	727324	4083530	-20
P1 -1400	727326	4083579	-18
P1 -1450	727328	4083629	-19
P1 -1500	727333	4083679	-20
P1 -1550	727331	4083729	-21
P1 -1600	727330.5	4083779	-22
P1 -1650	727330	4083828	-23
P1 -1700	727330	4083878	-24
P1 -1750	727330	4083929	-25
P1 -1800	727330	4083978	-26
P1 -1850	727334	4084027	-26
P1 -1900	727343	4084078	-27

P1 -1950	727349	4084130	-27
P1 -2000	727336	4084177	-29
Station	X (utm)	Y (utm)	Z_Mag
P2 750	725148	4082574	-21.0
P2 800	725148	4082624	-21.0
P2 850	725138	4082674	-20.0
P2 900	725129	4082723	-20.5
P2 925	725125	4082748	-20.8
P2 950	725121	4082772	-21.0
P2 975	725117	4082796	-20.8
P2 1000	725112	4082820	-20.5
P2 1025	725110	4082846	-19.8
P2 1050	725108	4082871	-19.0
P2 1075	725104	4082896	-18.8
P2 1100	725100	4082921	-18.5
P2 1125	725096	4082945	-18.3
P2 1150	725091	4082969	-18.0
P2 1175	725088	4082994	-18.0

P2 1200	725084	4083018	-18.0
P2 1225	725082	4083044	-18.5
P2 1250	725080	4083069	-19.0
P2 1300	725072	4083118	-19.0
P2 1350	725068	4083167	-19.0
P2 1400	725063	4083217	-18.0
P2 1450	725051	4083266	-17.0
P2 1500	725017	4083311	-19.0
P2 1550	725013	4083361	-19.0
P2 1600	725008	4083410	-20.0
P2 1650	724991	4083458	-19.0
P2 1700	724974	4083505	-19.0
P2 1750	724970	4083555	-21.0
P2 1800	724971	4083607	-20.0
P2 1850	724958	4083654	-20.0
P2 1900	724950	4083704	-21.0
P2 1950	724942	4083754	-23.0
P2 2000	724934	4083803	-22.0

P2 2050	724926	4083851	-23.0
Stations	X	Y	Z
P3 400	735348	4083945	-22
P3 450	735348	4083995	-22
P3 500	735348	4084045	-22
P3 550	735348	4084095	-22
P3 600	735362	4084144	-22
P3 650	735378	4084192	-22
P3 700	735388	4084241	-23
P3 750	735404	4084289	-23
P3 800	735411	4084338	-22
P3 850	735420	4084387	-23
P3 900	735420	4084438	-23
P3 950	735416	4084489	-23
P3 1000	735401	4084541	-24
P3 1050	735393	4084590	-23
P3 1100	735400	4084641	-23
P3 1150	735402	4084690	-22

P3 1200	735397	4084741	-23
P3 1250	735393	4084790	-23
P3 1300	735387	4084840	-24
P3 1350	735388	4084890	-23
P3 1400	735372	4084939	-24
P3 1450	735356	4084988	-25
P3 1500	735339	4085035	-26
P3 1550	735326	4085083	-26
P3 1600	735315	4085133	-25
P3 1650	735319	4085183	-25
P3 1700	735308	4085232	-25
P3 1750	735293	4085280	-27
P3 1800	735285	4085330	-26
P3 1850	735276	4085379	-26

Appendix B: Complete magnetometry profiles and other GPR sections

In this attachment, complete magnetometry profiles for profiles 1 to 3, whose anomalous areas were included in the report, are presented. Also, the processed sections of the parts of profile 2 that are not mentioned in the text of the report are presented in this appendix.

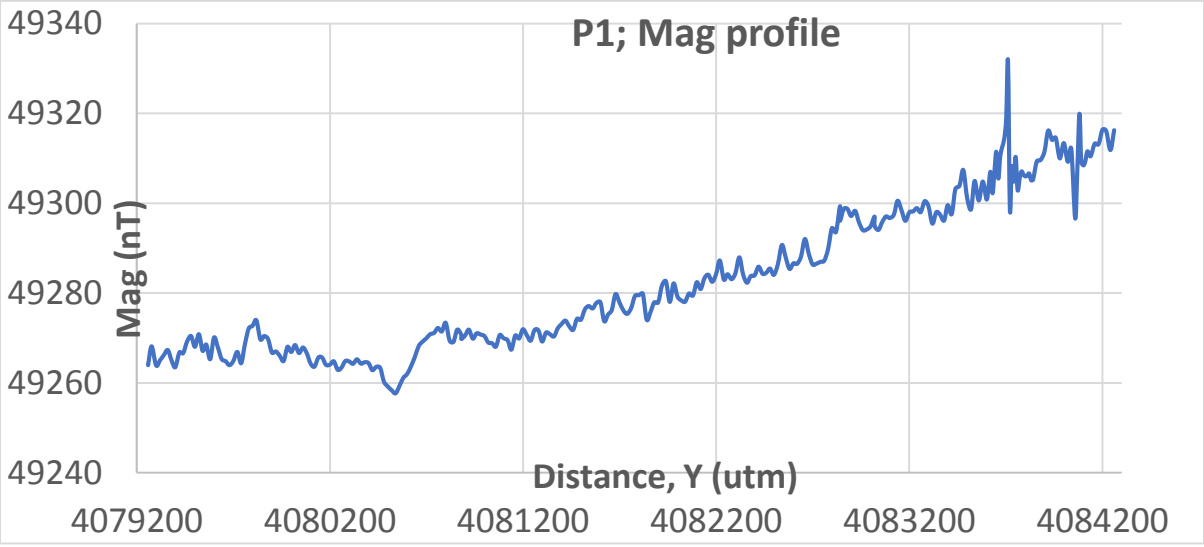

Figure B 1: The diagram of the total intensity of the magnetic field along profile 1, the horizontal axis, shows the Y position of the sampling stations in the UTM-WGS84 coordinate system.

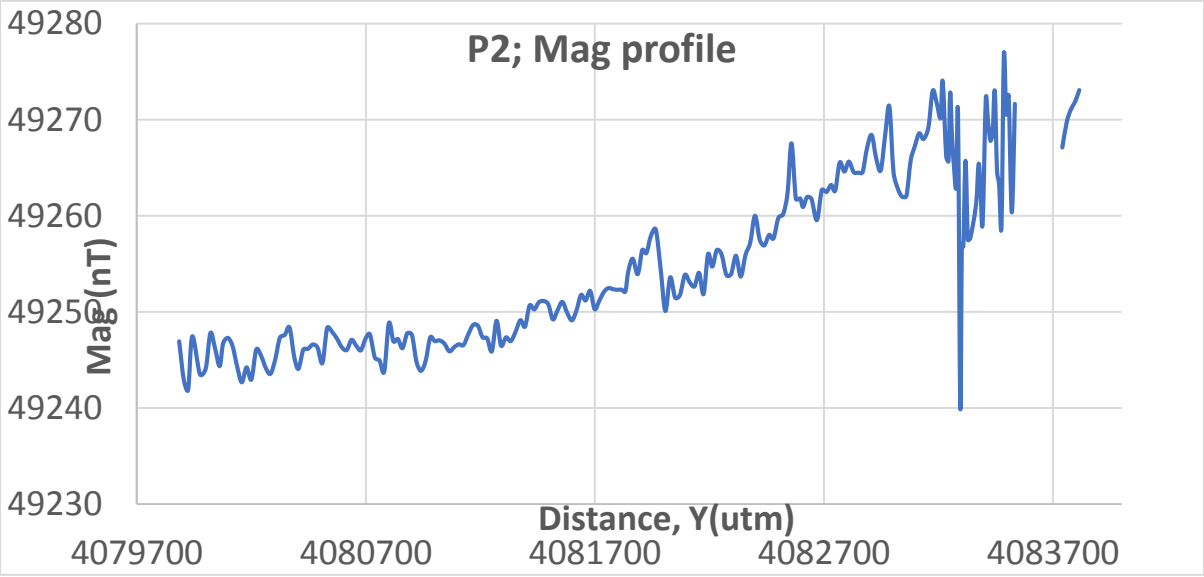

Figure B 2: The diagram of the total intensity of the magnetic field along profile 2, the horizontal axis, shows the Y position of the sampling stations in the UTM-WGS84 coordinate system.

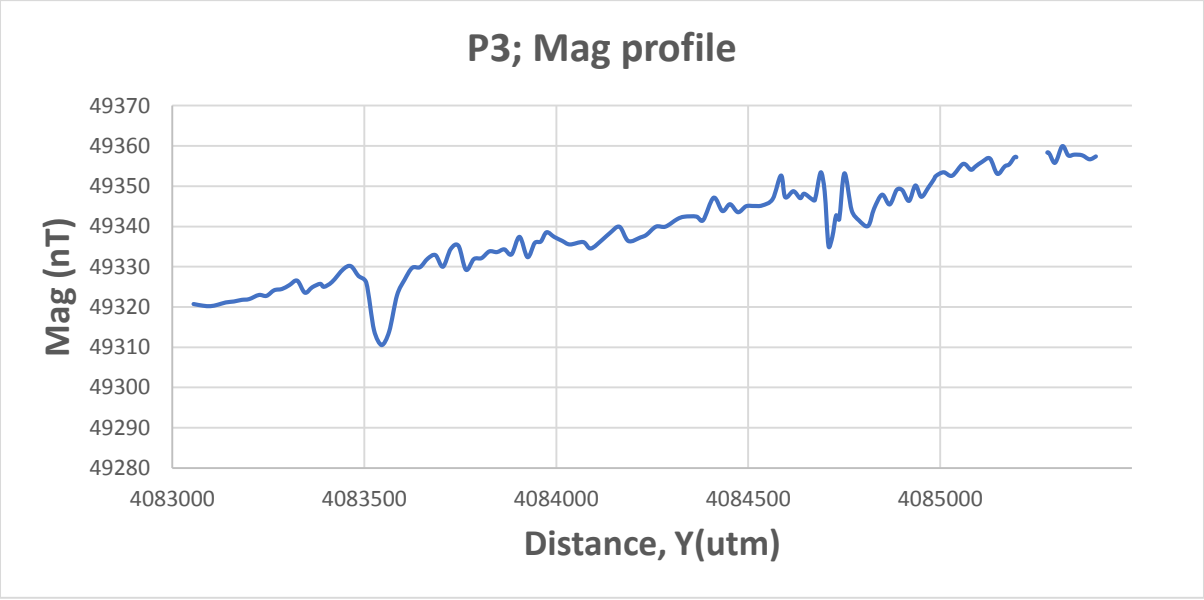

Figure B 3: The diagram of the total intensity of the magnetic field along profile 3, the horizontal axis, shows the Y position of the sampling stations in the UTM-WGS84 coordinate system.

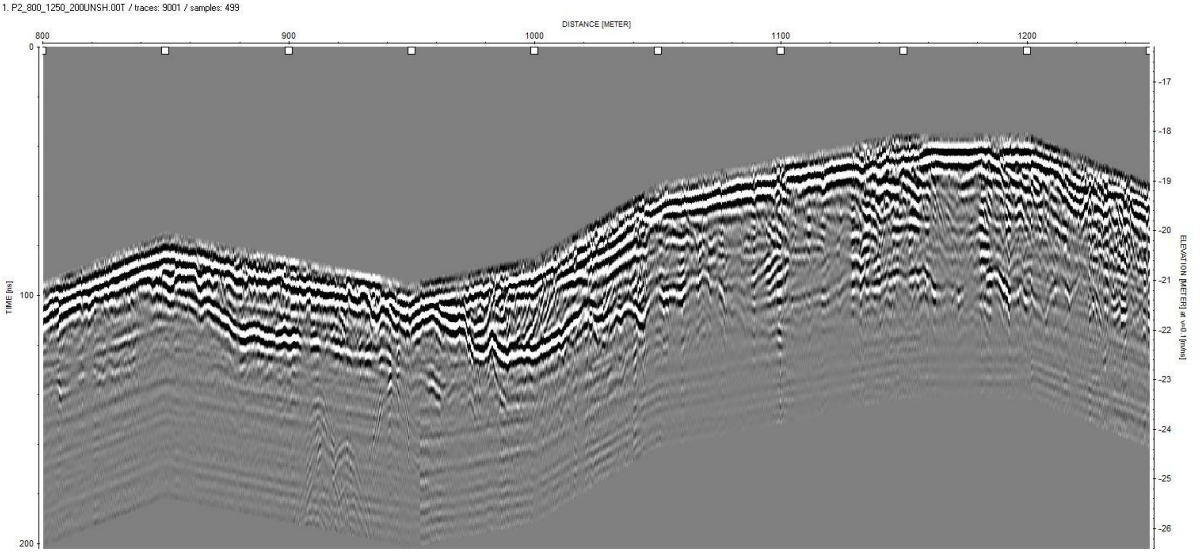

Figure B 4: Time and depth section (using an average velocity of 0.1 m/ns) processed GPR using an unshielded 200 MHz antenna and applying topography correction at station spacing 800 to 1250 profile 2.

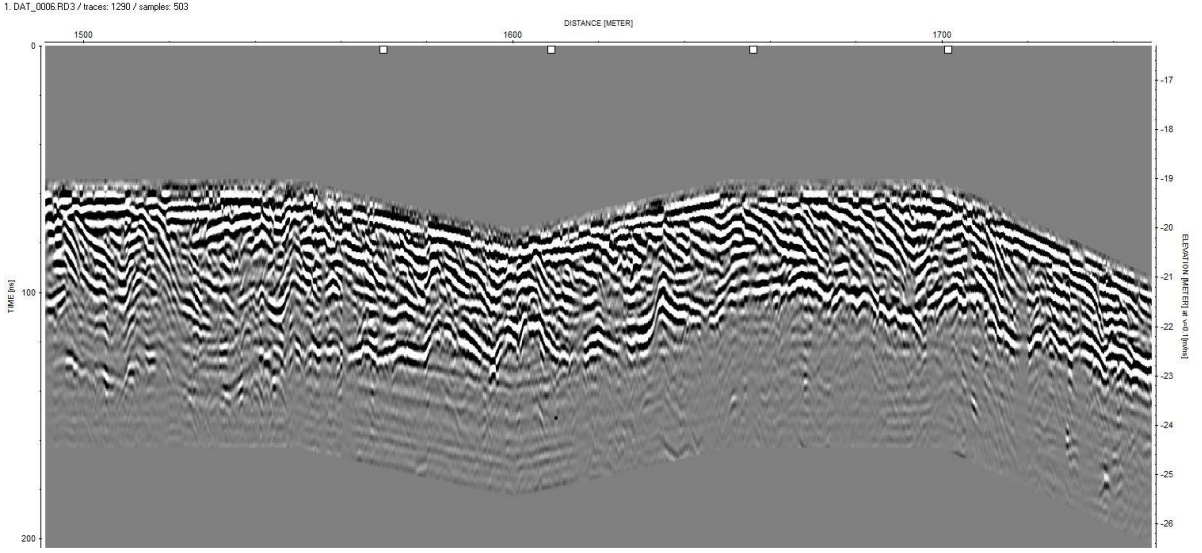

Figure B 5: Time and depth section (using average speed of 0.1 m/ns) processed GPR using 200 MHz unshielded antenna and applying topography correction at station distance 1490 to 1750 profile2

References:

Blakely, R.J., 1995. Potential theory in gravity and magnetic applications. Cambridge university press.

Ghasemi, Mohammadreza. and Mosavari, F., 2002, Geological map of Behshahr, scale 1:100000, Geological Survey of Iran

Telford, W. M., Geldart, L. P., & Sheriff, R. E. (1990). Applied geophysics. Cambridge university press.